Prog. Theor. Exp. Phys. **2021**, 013B03 (30 pages)
DOI: 10.1093/ptep/ptaa167

Revisiting the renormalization of Einstein–Maxwell theory at one-loop

I. Y. Park*

Department of Applied Mathematics, Philander Smith College, Little Rock, AR 72223, USA
*E-mail: inyongpark05@gmail.com

Received September 22, 2020; Revised November 3, 2020; Accepted November 15, 2020; Published November 19, 2020

In a series of recent works based on foliation-based quantization in which renormalizability has been achieved for the physical sector of the theory, we have shown that the use of the standard graviton propagator interferes, due to the presence of the trace mode, with the four-dimensional covariance. A subtlety in the background field method also requires careful handling. This status of the matter motivated us to revisit an Einstein-scalar system in one of the sequels. Continuing the endeavors, we revisit the one-loop renormalization of an Einstein–Maxwell system in the present work. The systematic renormalization of the cosmological and Newton constants is carried out by applying the refined background field method. The one-loop beta function of the vector coupling constant is explicitly computed and compared with the literature. The longstanding problem of the gauge choice dependence of the effective action is addressed, and the manner in which gauge choice independence is restored in the present framework is discussed. The formalism also sheds light on background independent analysis. The renormalization involves a metric field redefinition originally introduced by 't Hooft; with the field redefinition the theory should be predictive.

Subject Index B00, B05, B06, B32, B39

1. Introduction

A gravitational system (see, e.g., Refs. [1–6] for reviews) is much subtler and more complex than a non-gravitational one in many ways. This aspect is manifest in various forms, most notably in the challenges in quantization, which in turn have been spawning various obstructions. One can easily name several areas in which a firmer grasp of the quantization would better position one for a more complete treatment. Any study, and in particular the study of black hole information, in which the back reaction of the metric plays (or is expected to play) an important role, would be an example. The cosmological constant problem is also likely to benefit since it is the vacuum energy the complete understanding of which must be accompanied by handling of its quantum shift. Much of the difficulty in the quantization must be attributed to the large amount of gauge symmetry, the diffeomorphism. Therefore, one can reasonably expect that the key to the puzzle should lie largely in proper handling of the gauge symmetry. It has recently been realized that the diffeomorphism symmetry can be tamed, as depicted in Fig. 1, in a manner that accomplishes the renormalizability of gravity in its physical sector [7–9]; see Ref. [10] for a review. The renormalization procedures of pure Einstein gravity and an Einstein-scalar system have been carried out in the new quantization method in Refs. [11–13] and Refs. [14,15], respectively. We extend and expand those analyses to an Einstein–Maxwell system in this work.

The difficulties in a gravitational system could foster great opportunity, as, for instance, in holography, for understanding Nature. As is often the case (although nevertheless surprising if true), all

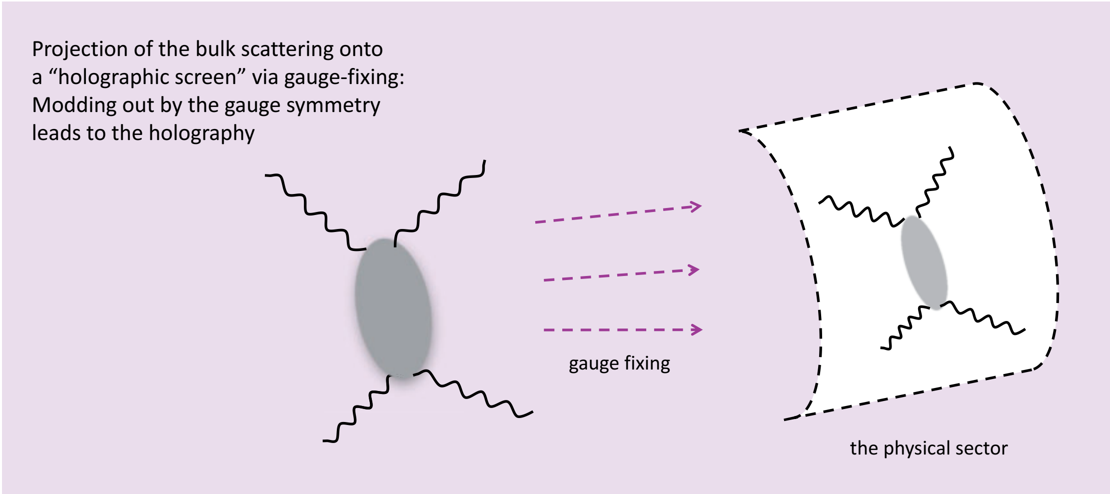

Fig. 1. Gauge-fixing-induced projection onto the physical states.

these different aspects may not be unrelated and may well in fact hinge closely on one another. Our recent works on gravity quantization were motivated by black hole information. While working on the quantization, we have come to realize that our understanding of the boundary conditions and dynamics is as yet incomplete; a more systematic and sound analysis of the boundary conditions needs to precede [16–19] a complete treatment of the quantization. As far as we are aware, its seriousness and importance have not, until recently, been accordingly stressed. (See the recent work by Witten, Ref. [20], for a discussion of the boundary conditions.) We have raised the possibility that information may be bleached through a quantum gravitational process in the vicinity of the horizon and released before the entry of the matter into the horizon [21,22]. The cosmological constant is generically generated by the loop effects [15], as will be reviewed below, and contributes to the generation of time-dependent solutions that in turn are linked with the black hole information [19].

Divergence analysis of an Einstein–Maxwell system was carried out long ago in an extensive work by Deser and van Nieuwenhuizen [23]. The counter-terms to the ultraviolet divergences were determined essentially by dimensional analysis and covariance. (The precise meaning of this statement is spelled out in footnote 6 by taking the simpler case considered in Ref. [24].) In our approach they are directly calculated in the Feynman diagrammatic method by employing the *traceless* propagator, as opposed to the widely used traceful propagator. (The need for a traceless propagator has been noted before [25–30].) This turns out to be crucial to avoid certain pathologies associated with the trace mode of the fluctuation metric: as explicitly demonstrated in Refs. [12,15], use of the standard graviton propagator interferes with the four-dimensional (4D) covariance. The results obtained complement the work of Ref. [23] in several aspects. We will also see, as a by-product, how the long-known gauge dependence issue related to that noted in Refs. [31–41] arises and is cleared up (at least) in the present framework.[1]

The analysis of an Einstein–Maxwell system carries considerable significance for our perspective. Firstly, the matter part itself is a gauge system and this poses additional hurdles (mentioned, e.g., in

[1] We deal with several different facets of the gauge choice dependence. One of the manifestations is well known, and has been extensively studied in the literature. Another is newly noted in the present framework. They will all be addressed in this paper.

footnote 7); overcoming them should constitute meaningful progress in the field. Secondly, it is in this work where the renormalization program using field redefinition is more thoroughly carried out: the focus of Ref. [15] was on establishing the *renormalizability* itself of a gravity–matter system. A more detailed and explicit analysis of, e.g., the running of the coupling constants was not conducted. In this work, the running of the cosmological constant and Newton's constant is addressed in much detail. Also, the one-loop beta function of the vector coupling constant is explicitly computed to demonstrate the power of the method. Since the renormalization involves a field redefinition, which is not necessary in the usual renormalizable theories, the explicit steps of the renormalization will be worth presenting; all of the required steps are taken in the present work. Further, the predictability of the theory, brought along by the renormalizability, is also explicitly addressed.

The paper is organized as follows. In Sect. 2 we outline the one-loop renormalization procedure in a general background metric $g_{\mu\nu}$ of the metric field equation. (Note that $g_{\mu\nu}$ denotes a solution, as opposed to the fluctuation denoted by $h_{\mu\nu}$ and background field by $\phi_{\mu\nu}$.) The analysis should make it clear that the methodology can be applied to an arbitrary solution $g_{\mu\nu}$. The first few relatively simple diagrams and their relevant vertices are identified. In Sect. 3.1 we carry out the explicit one-loop counter-term computation by taking $g_{\mu\nu} = \eta_{\mu\nu}$. A certain diagram yields a non-covariant expression and its inspection leads to a connection with the problem of certain novel gauge choice dependence[2] of the effective action. This particular gauge choice dependence is then resolved. The origin of the gauge choice dependence is found in Sect. 3.2 in the limitation of the background field method (BFM) in general, which can alternatively be viewed as a reflection of the complexity of a gravitational system. Afterwards, we look into how the well-known gauge choice dependence can be avoided as well. We end the section by noting that the freedom in choosing renormalization conditions is of great aid for facilitating background-independent analysis. In Sect. 4 we consider renormalization of the cosmological, Newton, and vector coupling constants. The vacuum-to-vacuum and tadpole diagrams are responsible for their renormalization. Unlike in a non-gravitational theory, the tadpole diagrams play a potentially important role. There are several technical subtleties, some of which have to do with dimensional regularization: the flat propagator yields vanishing results for the vacuum-to-vacuum and tadpole diagrams. The shifts in the coupling constants are introduced through finite renormalization. We show that the original Einstein–Hilbert action with the counter-terms can be rewritten as the same form of the Einstein–Hilbert action but now in terms of a redefined metric. An analysis of renormalization of the matter coupling was carried out in Refs. [39,40] by employing the setup of Ref. [37]. In the present work the beta function of the matter coupling is carried out by taking the cosmological constant as the graviton mass term as explained in the main body. The analysis yields the same result as Ref. [41]. Several ramifications, including the theory's predictability, are discussed. Section 5 contains a summary and future directions. We contemplate several possible procedures of renormalization. We also comment on the higher-loop extension of the present work.

2. Setup of loop computation

The preliminary step for renormalization and beta functions is to compute the one-particle-irreducible (1PI) effective action in the given background. (See, e.g., Refs. [3,42–44] for reviews of various

[2] This particular gauge choice dependence issue is new and not the same as the long-known one [31–34], although they have a similar origin. The latter dependence disappears by going on-shell [35,36]. The present framework elaborates on the on-shell disappearance; see Sect. 3.2.

methods of computing the effective action.) In this section we lay broader outlines of the counter-term computation in an arbitrary background, i.e. a solution of the metric field equation $g_{\mu\nu}$, before getting into the flat case in Sect. 3.1. (We will come back to the arbitrary metric case in Sect. 3.2.) We focus on several two-point amplitudes.

To carry out renormalization, one starts with the renormalized form of the Einstein–Maxwell action:

$$S = \int \sqrt{-\hat{g}_r}\left(\frac{1}{\kappa_r^2}\hat{R}_r - \frac{1}{4}\hat{F}^2_{r\mu\nu}\right), \tag{1}$$

where the renormalized quantities are indicated by the subscript r. For simplicity of the notation let us omit the subscript r:

$$S = \int \sqrt{-\hat{g}}\left(\frac{1}{\kappa^2}\hat{R} - \frac{1}{4}\hat{F}^2_{\mu\nu}\right). \tag{2}$$

For the BFM perturbative analysis, introduce the fluctuation fields $(h_{\mu\nu}, a_\mu)$ according to

$$\hat{g}_{\mu\nu} \equiv h_{\mu\nu} + \tilde{g}_{\mu\nu}, \qquad \hat{A}_\mu \equiv a_\mu + \tilde{A}_\mu. \tag{3}$$

The graviton propagator associated with the *traceless* fluctuation mode [7–9,12,13] (see also Ref. [45]) can be written as

$$\langle h_{\mu\nu}(x_1) h_{\rho\sigma}(x_2)\rangle = \tilde{P}_{\mu\nu\rho\sigma}\,\tilde{\Delta}(x_1 - x_2), \tag{4}$$

where the tensor $\tilde{P}_{\mu\nu\rho\sigma}$ is given by

$$\tilde{P}_{\mu\nu\rho\sigma} \equiv \frac{(2\kappa^2)}{2}\Big(\tilde{g}_{\mu\rho}\tilde{g}_{\nu\sigma} + \tilde{g}_{\mu\sigma}\tilde{g}_{\nu\rho} - \frac{1}{2}\tilde{g}_{\mu\nu}\tilde{g}_{\rho\sigma}\Big); \tag{5}$$

$\tilde{\Delta}(x_1 - x_2)$ is the Green's function for a scalar theory in the background metric $\tilde{g}_{\mu\nu}$. (There is, of course, the full propagator for the vector field; we will focus on the graviton sector.) The propagator almost exclusively used in the literature has a *trace piece*: instead of the coefficient $-1/2$ inside the parentheses in Eq. (5), the standard propagator has -1. As demonstrated in our previous works (e.g. Refs. [11,12,15]), the use of the traceful propagator destroys 4D covariance. As a matter of fact, the need for a traceless propagator has been observed before [25–30]. Our results explicitly demonstrate the pathology associated with the trace piece in the Feynman diagrammatic computation.

It turns out to be convenient to employ two different layers of perturbation. As we will see, it is possible to formally construct $\tilde{\Delta}(x_1 - x_2)$ in a closed-form; one may compute some of the diagrams by employing the full propagator in Eq. (4) (as well as the full propagator of the Maxwell sector), which we call the "first-layer" perturbation. (More on this "one-stroke" method later.) For other diagrams, in particular pure graviton diagrams, one may employ the "second-layer" perturbation[3] by splitting the $\tilde{g}$, $\tilde{A}_\mu$ appearing on the right-hand sides in Eq. (3) into

$$\tilde{g}_{\mu\nu} \equiv \varphi_{\mu\nu} + g_{\mu\nu}, \qquad \tilde{A}_\mu \equiv A_\mu + A_{0\mu}, \tag{6}$$

[3] For the one-loop effective action computation the present method correspond to perturbative expansion of the result obtained by applying the usual determinant formula, $\int D\xi\; e^{-\frac{1}{2}\xi K \xi} = e^{-\frac{1}{2}\mathrm{tr}\ln\frac{K}{2\pi}}$. The second-layer perturbation is not necessary in non-gravitational theories.

where $\varphi_{\mu\nu}, A_\mu$ represent the background fields and $g_{\mu\nu}, A_{0\mu}$ the classical solutions. (For instance, we will take $g_{\mu\nu} = \eta_{\mu\nu}, A_{0\mu} = 0$ in Sect. 3.) The shift with Eq. (6) was dubbed the "double-shift" in Ref. [12]. Essentially the same procedure was employed, though more implicitly, in Refs. [42–44]. The need for the second-layer perturbation for the gravity sector was discussed, e.g., in Refs. [11,12]. For most of the diagrams that we will consider, the structures of the vertices allow one to approximate $\tilde{P}_{\mu\nu\rho\sigma}$ for the given order,

$$\tilde{P}_{\mu\nu\rho\sigma} \simeq P_{\mu\nu\rho\sigma} \equiv \frac{(2\kappa^2)}{2}\Big(g_{\mu\rho}g_{\nu\sigma} + g_{\mu\sigma}g_{\nu\rho} - \frac{1}{2}g_{\mu\nu}g_{\rho\sigma}\Big), \tag{7}$$

where $P_{\mu\nu\rho\sigma}$ is the leading-order $\varphi_{\mu\nu}$-expansion of $\tilde{P}_{\mu\nu\rho\sigma}$. We will also see the use of the full tensor $\tilde{P}_{\mu\nu\rho\sigma}$ in some of the computations, the first-layer perturbation examples. For the divergence analysis one can use $\tilde{\Delta}(x_1 - x_2) \simeq \Delta(x_1 - x_2)$, where $\Delta(x_1 - x_2)$ denotes the scalar propagator for $g_{\mu\nu} = \eta_{\mu\nu}$,

$$\Delta(x_1 - x_2) = \int \frac{d^4k}{(2\pi)^4}\frac{e^{ik\cdot(x_1-x_2)}}{ik^2}. \tag{8}$$

In this "bottom-up" approach, the quantities that one intends to calculate in the first-layer perturbation can be calculated through the second-layer perturbation. Dimensional analysis and the 4D covariance provide useful consistency checks, as will be demonstrated in Sect. 3.

Let us expand the action in terms of the fluctuation fields $h_{\mu\nu}, a_\mu$. Including the gauge-fixing and ghost terms, one gets

$$S = \int \Big(\frac{1}{\kappa^2}\mathcal{L}_{\text{grav}} + \mathcal{L}_{\text{matter}}\Big), \tag{9}$$

where[4]

$$\begin{aligned}
\kappa^2\mathcal{L}_{\text{grav}} = \frac{1}{2}\sqrt{-\tilde{g}}\Big(&-\frac{1}{2}\tilde{\nabla}_\gamma h^{\alpha\beta}\tilde{\nabla}^\gamma h_{\alpha\beta} + \frac{1}{4}\tilde{\nabla}_\gamma h^\alpha_\alpha \tilde{\nabla}^\gamma h^\beta_\beta \\
&+ h_{\alpha\beta}h_{\gamma\delta}\tilde{R}^{\alpha\gamma\beta\delta} - h_{\alpha\beta}h^\beta{}_\gamma\tilde{R}^{\kappa\alpha\gamma}{}_\kappa - h^\alpha{}_\alpha h_{\beta\gamma}\tilde{R}^{\beta\gamma} - \frac{1}{2}h^{\alpha\beta}h_{\alpha\beta}\tilde{R} + \frac{1}{4}h^\alpha_\alpha h^\beta_\beta\tilde{R} + \cdots\Big) \\
&- \tilde{\nabla}^\nu\bar{C}^\mu\tilde{\nabla}_\nu C_\mu + \tilde{R}_{\mu\nu}\bar{C}^\mu C^\nu - \omega^*\tilde{\nabla}^\mu\tilde{F}_{\mu\nu}C^\nu - \omega^*\tilde{F}_{\mu\nu}\tilde{\nabla}^\mu C^\nu + \cdots
\end{aligned} \tag{10}$$

and

$$\begin{aligned}
\mathcal{L}_{\text{matter}} = -\frac{1}{4}\sqrt{-\tilde{g}}\Big[&\tilde{g}^{\mu\nu}\tilde{g}^{\rho\sigma} - \tilde{g}^{\mu\nu}h^{\rho\sigma} - \tilde{g}^{\rho\sigma}h^{\mu\nu} + \frac{1}{2}\tilde{g}^{\mu\nu}\tilde{g}^{\rho\sigma}h + \tilde{g}^{\mu\nu}h^{\rho\kappa}h^\sigma_\kappa + \tilde{g}^{\rho\sigma}h^{\mu\kappa}h^\nu_\kappa \\
&- \frac{1}{2}\tilde{g}^{\mu\nu}hh^{\rho\sigma} - \frac{1}{2}\tilde{g}^{\rho\sigma}hh^{\mu\nu} + h^{\mu\nu}h^{\rho\sigma} + \frac{1}{8}\tilde{g}^{\mu\nu}\tilde{g}^{\rho\sigma}(h^2 - 2h_{\kappa_1\kappa_2}h^{\kappa_1\kappa_2})\Big]\big(f_{\mu\rho}f_{\nu\sigma} + 2f_{\mu\rho}\tilde{F}_{\nu\sigma} + \tilde{F}_{\mu\rho}\tilde{F}_{\nu\sigma}\big) \\
&- \frac{1}{2}\sqrt{-\tilde{g}}\,(\tilde{\nabla}_\kappa a^\kappa)^2 - \tilde{\nabla}\omega^*\tilde{\nabla}\omega + \cdots,
\end{aligned} \tag{11}$$

where the raising and lowering are done by $\tilde{g}^{\mu\nu}$ and $\tilde{g}_{\mu\nu}$, respectively. Above, (C^κ, ω) are the ghosts for the diffeomorphism and vector gauge transformation, respectively.[5] Putting it all together, Eq. (9)

---

[4] The $\tilde{R}_{\mu\nu}\bar{C}^\mu C^\nu$ term of the gravity sector action $\mathcal{L}_{\text{grav}}$ presented in Ref. [15] has a sign error due to mixed conventions. Both this term and the affected equations have been corrected in Ref. [12].

[5] These ghost terms correspond to the following transformations of the fluctuation fields [23]:

$$h'_{\mu\nu} = h_{\mu\nu} + (\tilde{g}_{\mu\kappa}\tilde{D}_\nu + \tilde{g}_{\nu\kappa}\tilde{D}_\mu)\eta^\kappa + (h_{\mu\kappa}\tilde{D}_\nu + h_{\nu\kappa}\tilde{D}_\mu)\eta^\kappa + \eta^\kappa\tilde{D}_\kappa h^{\mu\nu},$$

can be written in a more useful form as the sum of the kinetic part and the vertices:

$$S \equiv S_{\rm k} + S_{\rm v}, \tag{12}$$

with

$$S_{\rm k} = \int \sqrt{-\tilde{g}}\, \frac{1}{2\kappa^2}\Big(-\frac{1}{2}\tilde{\nabla}_\gamma h^{\alpha\beta}\tilde{\nabla}^\gamma h_{\alpha\beta} + \frac{1}{4}\tilde{\nabla}_\gamma h^\alpha_\alpha \tilde{\nabla}^\gamma h^\beta_\beta \Big) - \frac{1}{4}\sqrt{-\tilde{g}}\,\left(\tilde{g}^{\mu\nu}\tilde{g}^{\rho\sigma} f_{\mu\rho} f_{\nu\sigma}\right)$$
$$- \frac{1}{2}\sqrt{-\tilde{g}}\,(\tilde{\nabla}_\kappa a^\kappa)^2 + \frac{1}{2\kappa^2}\sqrt{-\tilde{g}}\,(-\tilde{\nabla}^\nu \bar{C}^\mu \tilde{\nabla}_\nu C_\mu) - \sqrt{-\tilde{g}}\,\tilde{\nabla}^\rho \omega^* \tilde{\nabla}_\rho \omega \tag{13}$$

and

$$S_{\rm v} = \int \sqrt{-\tilde{g}}\, \frac{1}{2\kappa^2}\Big(h_{\alpha\beta}h_{\gamma\delta}\tilde{R}^{\alpha\gamma\beta\delta} - h_{\alpha\beta}h^\beta{}_\gamma \tilde{R}^{\kappa\alpha\gamma}{}_\kappa - h^\alpha{}_\alpha h_{\beta\gamma}\tilde{R}^{\beta\gamma} - \frac{1}{2}h^{\alpha\beta}h_{\alpha\beta}\tilde{R}$$
$$+ \frac{1}{4}h^\alpha_\alpha h^\beta_\beta \tilde{R}\Big) - \frac{1}{4}\sqrt{-\tilde{g}}(\tilde{g}^{\mu\nu}\tilde{g}^{\rho\sigma})\big(+2f_{\mu\rho}\tilde{F}_{\nu\sigma} + \tilde{F}_{\mu\rho}\tilde{F}_{\nu\sigma}\big) - \frac{1}{4}\sqrt{-\tilde{g}}\Big[-\tilde{g}^{\mu\nu}h^{\rho\sigma}$$
$$-\tilde{g}^{\rho\sigma}h^{\mu\nu} + \frac{1}{2}\tilde{g}^{\mu\nu}\tilde{g}^{\rho\sigma}h + \tilde{g}^{\mu\nu}h^{\rho\kappa}h^\sigma_\kappa + \tilde{g}^{\rho\sigma}h^{\mu\kappa}h^\nu_\kappa - \frac{1}{2}\tilde{g}^{\mu\nu}hh^{\rho\sigma} - \frac{1}{2}\tilde{g}^{\rho\sigma}hh^{\mu\nu}$$
$$+ h^{\mu\nu}h^{\rho\sigma} + \frac{1}{8}\tilde{g}^{\mu\nu}\tilde{g}^{\rho\sigma}(h^2 - 2h_{\kappa_1\kappa_2}h^{\kappa_1\kappa_2})\Big]\big(f_{\mu\rho}f_{\nu\sigma} + 2f_{\mu\rho}\tilde{F}_{\nu\sigma} + \tilde{F}_{\mu\rho}\tilde{F}_{\nu\sigma}\big)$$
$$+ \frac{1}{2\kappa^2}\sqrt{-\tilde{g}}\,\left(\tilde{R}_{\mu\nu}\bar{C}^\mu C^\nu + \frac{1}{2}\tilde{\nabla}^\mu \omega^* \tilde{F}_{\mu\nu}C^\nu\right) + \cdots . \tag{14}$$

2.1. *On the gauge fixing*

A crucial feature of the action above, which has been set up for the refined BFM, is how the graviton gauge fixing has been implemented:

$$-\frac{1}{2}\left[\tilde{\nabla}_\nu h^{\mu\nu} - \frac{1}{2}\tilde{\nabla}^\mu h\right]^2. \tag{15}$$

This is the refined BFM version of the usual gauge fixing,

$$-\frac{1}{2}\left[\nabla_\nu h^{\mu\nu} - \frac{1}{2}\nabla^\mu h\right]^2 \tag{16}$$

that is $\tilde{g}_{\mu\nu}$-background non-covariant. In other words, one starts with Eq. (16) and converts it into Eq. (15) when turning to the refined BFM. The physical content of the gauge condition satisfied by $h_{\mu\nu}$ is still Eq. (16) since the BFM is just a convenience device that allows one to conduct the analysis more covariantly than otherwise. (The field $\varphi_{\mu\nu}$ satisfies the same gauge fixing; see footnote 9 below.) Naively, one expects that with the gauge fixing in Eq. (15) the 1PI effective action will come out to be $\tilde{g}_{\mu\nu}$-covariant. Later we will see that the 1PI action is non-covariant due to the presence of the terms that can be removed by enforcing the strong form of the gauge condition, which provides an important clue as to how to solve this particular gauge choice dependence of the effective action.

$$a'_\mu = a_\mu + \eta^\kappa \tilde{F}_{\kappa\mu} + \tilde{D}_\mu \eta^5 + a_\kappa \tilde{D}_\mu \eta^\mu + \eta^\kappa \tilde{D}_\kappa a_\mu$$

under $x'^\alpha = x^\alpha - \eta^\alpha$ and the vector gauge transformation with the parameter $-\eta^\kappa \tilde{A}_\kappa + \eta^5$.

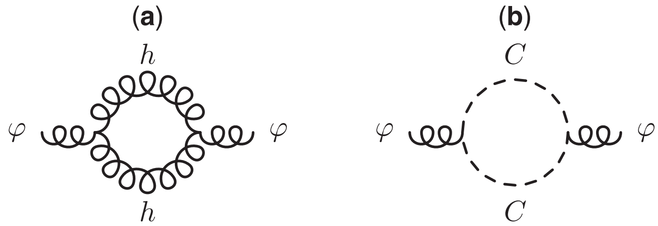

Fig. 2. Graviton and ghost diagrams (indices on fields suppressed).

2.2. Two-point diagrams

In general, the renormalization in a curved background $g_{\mu\nu}$ is technically involved. It is nevertheless possible to outline the steps of the amplitude computation for an arbitrary solution metric $g_{\mu\nu}$.

Cautionary remarks are in order. It is important to distinguish the second-layer diagrams from the first-layer ones. Only the first-layer diagrams will individually yield covariant results. A given first-layer diagram corresponds, in general, to multiple second-layer diagrams even at a fixed order of $\varphi_{\mu\nu}$. Consider, for example, the graviton kinetic action,

$$\mathcal{L}_{\text{grav,kin}} = \frac{1}{2\kappa^2}\sqrt{-\tilde{g}}\left(-\frac{1}{2}\tilde{\nabla}_\gamma h^{\alpha\beta}\tilde{\nabla}^\gamma h_{\alpha\beta} + \frac{1}{4}\tilde{\nabla}_\gamma h^\alpha_\alpha \tilde{\nabla}^\gamma h^\beta_\beta \right), \tag{17}$$

and the one-loop vacuum-to-vacuum amplitude. Although there is a unique one-loop vacuum-to-vacuum amplitude, , in the first-layer perturbation, the diagram corresponds to multiple second-layer ones. At the second order in $\varphi_{\alpha\beta}$, the relevant diagram is the one given in Fig. 2(a). More on this as we continue.

With the split given in Eq. (6), the kinetic terms themselves yield the vertices for the second-layer perturbation expansion. For instance, the graviton kinetic term is expanded as

$$\begin{aligned} 2\kappa^2\mathcal{L}_{\text{grav,kin}} = &-\frac{1}{2}\partial_\gamma h^{\alpha\beta}\partial^\gamma h_{\alpha\beta} + \frac{1}{4}\partial_\gamma h^\alpha_\alpha \partial^\gamma h^\beta_\beta + \Big\{ \big(2g^{\beta\beta'}\tilde{\Gamma}^{\alpha'\gamma\alpha} - g^{\alpha\beta}\tilde{\Gamma}^{\alpha'\gamma\beta'}\big)\partial_\gamma h_{\alpha\beta}\, h_{\alpha'\beta'} \\ &+ \Big[\frac{1}{2}\big(g^{\alpha\alpha'}g^{\beta\beta'}\varphi^{\gamma\gamma'} + g^{\beta\beta'}g^{\gamma\gamma'}\varphi^{\alpha\alpha'} + g^{\alpha\alpha'}g^{\gamma\gamma'}\varphi^{\beta\beta'}\big) - \frac{1}{4}\varphi\, g^{\alpha\alpha'}g^{\beta\beta'}g^{\gamma\gamma'} \\ &- \frac{1}{2}g^{\gamma\gamma'}g^{\alpha'\beta'}\varphi^{\alpha\beta} + \frac{1}{4}\Big(-\varphi^{\gamma\gamma'} + \frac{1}{2}\varphi g^{\gamma\gamma'}\Big) g^{\alpha\beta}g^{\alpha'\beta'}\Big]\partial_\gamma h_{\alpha\beta}\,\partial_{\gamma'} h_{\alpha'\beta'}\Big\}, \end{aligned} \tag{18}$$

where the raising and lowering are done by $g^{\mu\nu}$ and $g_{\mu\nu}$, respectively. The terms within the gray braces serve as the vertices responsible for Fig. 2(a). The corresponding ghost diagram is given in Fig. 2(b).

The forms of all possible second-layer vertices can be obtained by applying this scheme to the rest of the terms in Eqs. (13) and (14). The first several relatively simple matter-involving diagrams are listed in Fig. 2. In general, we restrict the maximum number of graviton external lines to two for simplicity. Overall, the diagrams are classified into four categories. The first class is the diagrams with both vertices from the graviton sector: the pure gravity sector two-point amplitude and the corresponding ghost-loop diagram in Fig. 2. They were considered in Ref. [12] and will be reviewed below. The second class is the diagrams with both vertices from the matter sector, Fig. 3(a)–(c). The third is the diagrams with one vertex from the graviton sector and the other from the matter sector, Fig. 3(d).

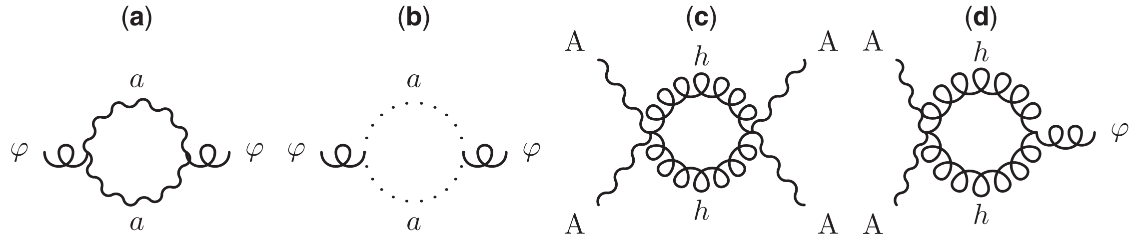

Fig. 3. Matter-involving diagrams.

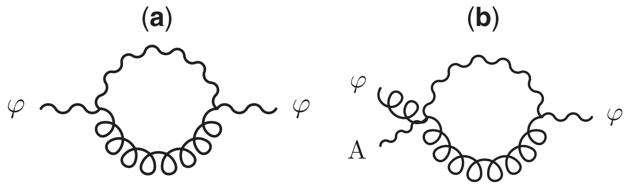

Fig. 4. Diagrams with inhomogeneous loops.

All of the diagrams so far have had "homogeneous" loops, whereas the diagrams in Fig. 4 have "inhomogeneous" or "heterotic" ones. They are classified as the fourth class due to the fact that they require special care.

The vertex, V_g, responsible for the diagrams in Fig. 2(a) is defined by rewriting Eq. (18) as

$$\mathcal{L} = \frac{1}{\kappa'^2}\left[-\frac{1}{2}\partial_\gamma h^{\alpha\beta}\partial^\gamma h_{\alpha\beta} + \frac{1}{4}\partial_\gamma h^\alpha_\alpha \partial^\gamma h^\beta_\beta + \mathcal{L}_{V_g}\right], \tag{19}$$

where $\kappa'^2 \equiv 2\kappa^2$ and

$$\begin{aligned} V_g \equiv{}& \sqrt{-g}\big(2g^{\beta\beta'}\tilde{\Gamma}^{\alpha'\gamma\alpha} - g^{\alpha\beta}\tilde{\Gamma}^{\alpha'\gamma\beta'}\big)\partial_\gamma h_{\alpha\beta}\, h_{\alpha'\beta'} + \sqrt{-g}\bigg[\frac{1}{2}\big(g^{\alpha\alpha'}g^{\beta\beta'}\varphi^{\gamma\gamma'} + g^{\beta\beta'}g^{\gamma\gamma'}\varphi^{\alpha\alpha'} \\ &+ g^{\alpha\alpha'}g^{\gamma\gamma'}\varphi^{\beta\beta'}\big) - \frac{1}{4}\varphi\, g^{\alpha\alpha'}g^{\beta\beta'}g^{\gamma\gamma'} - \frac{1}{2}g^{\gamma\gamma'}g^{\alpha'\beta'}\varphi^{\alpha\beta} \\ &+ \frac{1}{4}\Big(-\varphi^{\gamma\gamma'} + \frac{1}{2}\varphi g^{\gamma\gamma'}\Big)g^{\alpha\beta}g^{\alpha'\beta'}\bigg]\partial_\gamma h_{\alpha\beta}\,\partial_{\gamma'} h_{\alpha'\beta'} \\ &+ \sqrt{-\tilde{g}}\Big(h_{\alpha\beta}h_{\gamma\delta}\tilde{R}^{\alpha\gamma\beta\delta} - h_{\alpha\beta}h^\beta{}_\gamma \tilde{R}^{\kappa\alpha\gamma}{}_\kappa - h^\alpha{}_\alpha h_{\beta\gamma}\tilde{R}^{\beta\gamma} - \frac{1}{2}h^{\alpha\beta}h_{\alpha\beta}\tilde{R} + \frac{1}{4}h^\alpha_\alpha h^\beta_\beta \tilde{R}\Big). \end{aligned} \tag{20}$$

$\mathcal{L}_{V_g}$ appearing in Eq. (19) and V_g are related by $V_g = \sqrt{-g}\,\mathcal{L}_{V_g}$. As for $\tilde{g}_{\mu\nu}$-containing quantities, expansion in terms of $\varphi_{\mu\nu}$ is to be understood.

The vertex responsible for the ghost-loop diagram can be similarly identified by expanding the terms quadratic in the ghost field:

$$\begin{aligned} V_C \equiv -\sqrt{-g}\bigg[&\frac{1}{2}\varphi\partial^\mu \bar{C}^\nu \partial_\mu C_\nu - \tilde{\Gamma}^\lambda_{\mu\nu}(\partial^\mu \bar{C}^\nu C_\lambda - \partial^\mu C^\nu \bar{C}_\lambda) \\ &- (g^{\nu\beta}\varphi^{\mu\alpha} + g^{\mu\alpha}\varphi^{\nu\beta})\partial_\beta \bar{C}_\alpha \partial_\nu C_\mu\bigg] + \sqrt{-g}\, R_{\mu\nu}\bar{C}^\mu C^\nu. \end{aligned} \tag{21}$$

The vertices responsible for the diagrams in Figs. 3 and 4 can be similarly obtained by examining the matter part of the action (the trace piece $h \equiv \tilde{g}^{\alpha\beta} h_{\alpha\beta}$ has been set to zero [7–9,12,13]):

$$
\begin{aligned}
V_{m1} &\equiv -\frac{1}{4}\sqrt{-g}\left[-g^{\rho\sigma}\varphi^{\mu\nu} - g^{\mu\nu}\varphi^{\rho\sigma}\right] f_{\mu\rho} f_{\nu\sigma},\\
V_{m2} &\equiv -\frac{1}{4}\sqrt{-g}\left[g^{\mu\nu}h^{\rho\kappa}h_{\kappa}^{\sigma} + g^{\rho\sigma}h^{\mu\kappa}h_{\kappa}^{\nu} + h^{\mu\nu}h^{\rho\sigma} - \frac{1}{4}g^{\mu\nu}g^{\rho\sigma}h_{\kappa_1\kappa_2}h^{\kappa_1\kappa_2}\right]\tilde{F}_{\mu\rho}\tilde{F}_{\nu\sigma},\\
V_{m3} &\equiv \frac{1}{2}\sqrt{-g}\left[g^{\mu\nu}h^{\rho\sigma} + g^{\rho\sigma}h^{\mu\nu}\right] f_{\mu\rho} F_{\nu\sigma},\\
V_{m4} &\equiv -\frac{1}{2}\sqrt{-g}\left[\varphi^{\mu\nu}h^{\rho\sigma} + \varphi^{\rho\sigma}h^{\mu\nu}\right] f_{\mu\rho} F_{\nu\sigma}.
\end{aligned}
\tag{22}
$$

Let us work out the counter-terms to the diagrams in Figs. 2–4. Below, $\Rightarrow$ means that the diagram on the left-hand side leads to the counter-term(s) on the right-hand side. The graviton and ghost contributions respectively are

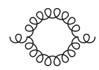

$$
\Rightarrow -\frac{1}{2}\frac{1}{\kappa'^4}\left\langle\left(\int V_g\right)^2\right\rangle,
\tag{23}
$$

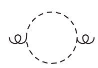

$$
\Rightarrow -\frac{1}{2}\frac{1}{\kappa'^4}\left\langle\left(\int V_C\right)^2\right\rangle.
\tag{24}
$$

The numerical factors of $-\frac{1}{2}$ are the combinatoric factors that arise when the vertices are brought down from the exponent in the path integral. The total gravity sector one-loop counter-terms are given by the sum of these two; the result for the flat case was obtained in Ref. [12] and will be quoted in Sect. 3.

The diagrams in Fig. 3(a) and (c) have two vertices, V_{m1} and V_{m2}, inserted respectively; one gets

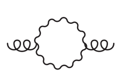

$$
\Rightarrow -\frac{1}{2}\left\langle\left(\int V_{m1}\right)^2\right\rangle = -\frac{1}{2}\left\langle\left[\int \frac{1}{4}(g^{\rho\sigma}\varphi^{\mu\nu} + g^{\mu\nu}\varphi^{\rho\sigma})(f_{\mu\rho}f_{\nu\sigma})\right]^2\right\rangle,
\tag{25}
$$

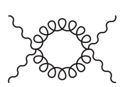

$$
\begin{aligned}
\Rightarrow -\frac{1}{2}\left\langle\left(\int V_{m2}\right)^2\right\rangle = -\frac{1}{2}\Bigg\langle\Bigg[\int \frac{1}{4}\Bigg(&g^{\mu\nu}h^{\rho\kappa}h_{\kappa}^{\sigma} + g^{\rho\sigma}h^{\mu\kappa}h_{\kappa}^{\nu} + h^{\mu\nu}h^{\rho\sigma}\\
&-\frac{1}{4}g^{\mu\nu}g^{\rho\sigma}h_{\kappa_1\kappa_2}h^{\kappa_1\kappa_2}\Bigg)(\tilde{F}_{\mu\rho}\tilde{F}_{\nu\sigma})\Bigg]^2\Bigg\rangle.
\end{aligned}
\tag{26}
$$

The cross-term diagram in Fig. 3(d) is generated by the vacuum expectation value of the two vertices, one of which is the matter vertex V_{m_2} and the other V_g. The diagram corresponds to

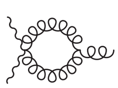

$$
\begin{aligned}
&\Rightarrow -\left\langle\int V_{m2}\int V_g\right\rangle\\
&= -\left\langle\int\left(-\frac{1}{4}\right)\left[g^{\mu\nu}h^{\rho\kappa}h_{\kappa}^{\sigma} + g^{\rho\sigma}h^{\mu\kappa}h_{\kappa}^{\nu} + h^{\mu\nu}h^{\rho\sigma} - \frac{1}{4}g^{\mu\nu}g^{\mu\nu}h_{\kappa_1\kappa_2}h^{\kappa_1\kappa_2}\right](\tilde{F}_{\mu\rho}\tilde{F}_{\nu\sigma})\right.\\
&\qquad \times \frac{1}{\kappa'^2}\int\Big\{(2g^{\beta\beta'}\tilde{\Gamma}^{\alpha'\gamma\alpha} - g^{\alpha\beta}\tilde{\Gamma}^{\alpha'\gamma\beta'})\partial_\gamma h_{\alpha\beta}\, h_{\alpha'\beta'}
\end{aligned}
$$

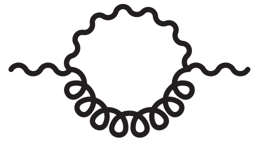

Fig. 5. First-layer perturbation diagram.

$$
\begin{aligned}
&+\bigg[\frac{1}{2}(g^{\alpha\alpha'}g^{\beta\beta'}\varphi^{\gamma\gamma'}+g^{\beta\beta'}g^{\gamma\gamma'}\varphi^{\alpha\alpha'}+g^{\alpha\alpha'}g^{\gamma\gamma'}\varphi^{\beta\beta'})-\frac{1}{2}g^{\gamma\gamma'}g^{\alpha'\beta'}\varphi^{\alpha\beta}\\
&\quad-\frac{1}{4}\varphi^{\gamma\gamma'}g^{\alpha\beta}g^{\alpha'\beta'}\bigg]\partial_\gamma h_{\alpha\beta}\,\partial_{\gamma'}h_{\alpha'\beta'}\\
&+\left(h_{\alpha\beta}h_{\gamma\delta}\tilde{R}^{\alpha\gamma\beta\delta}-h_{\alpha\beta}h^{\beta}{}_{\gamma}\tilde{R}^{\kappa\alpha\gamma}{}_{\kappa}-\frac{1}{2}h^{\alpha\beta}h_{\alpha\beta}\tilde{R}\right)\bigg\}\bigg\rangle. \qquad (27)
\end{aligned}
$$

The computation of the diagrams with the heterotic loops serves as an example of the first-layer perturbation. For them it is necessary to use the full propagator in Eq. (4), a step not needed for the other diagrams so far for a structural reason. In the first-layer perturbation, the graph to calculate is shown in Fig. 5. Note that unlike Fig. 4(a), the lines have been thickened. The external lines represent the full fields, i.e. the fields with tildes; see Eq. (6). By the same token, the internal lines represent the full propagators. (The two diagrams in Fig. 4 are the first two terms that result from, so to speak, $\varphi_{\alpha\beta}$-expanding the graph in Fig. 5. There are additional contributions coming from the internal lines when the full propagators are used.) As for the diagrams in Fig. 4, they can be set up in a manner similar to the others:

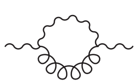

$$
\Rightarrow -\frac{1}{2}\left\langle\left(\int V_{m3}\right)^2\right\rangle=-\frac{1}{2}\left\langle\left(\int\frac{1}{2}(g^{\mu\nu}h^{\rho\sigma}+g^{\rho\sigma}h^{\mu\nu})f_{\mu\rho}F_{\nu\sigma}\right)^2\right\rangle,
$$

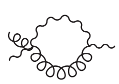

$$
\begin{aligned}
\Rightarrow -\left\langle\int V_{m3}\int V_{m4}\right\rangle&=-\bigg\langle\int\frac{1}{2}(g^{\mu\nu}h^{\rho\sigma}+g^{\rho\sigma}h^{\mu\nu})f_{\mu\rho}F_{\nu\sigma}\\
&\quad\times\int\frac{-1}{2}(\varphi^{\mu'\nu'}h^{\rho'\sigma'}+\varphi^{\rho'\sigma'}h^{\mu'\nu'})f_{\mu'\rho'}F_{\nu'\sigma'}\bigg\rangle. \qquad (28)
\end{aligned}
$$

We will leave it for now and come back in Sect. 3 where we show a more convenient way of effectively calculating all the contributions, including those arising from the full internal propagators.

2.3. *Vacuum-to-vacuum and tadpole diagrams*

In the first-layer perturbation, the shifts in the cosmological and Newton constants are caused by the vacuum-to-vacuum and tadpole diagrams, respectively (more details in Sect. 4). Figure 6 lists the diagrams for the pure gravity sector; there are similar diagrams for the matter-involving sector. For the graviton vacuum-to-vacuum amplitude, for example, one is to compute

$$
\int\prod_x dh_{\kappa_1\kappa_2}\ \exp\left\{\frac{i}{\kappa'^2}\int\sqrt{-\tilde{g}}\left(-\frac{1}{2}\tilde{\nabla}_\gamma h^{\alpha\beta}\tilde{\nabla}^\gamma h_{\alpha\beta}\right)\right\}. \qquad (29)
$$

This vacuum energy amplitude in the first-layer perturbation will give a vacuum diagram and a tadpole diagram in the second layer. As for the vector coupling renormalization, the relevant diagram is given in Fig. 7, a tadpole diagram with the graviton running on the loop. The relevant first-layer vertex is

$$
-\frac{1}{4}\int\sqrt{-\tilde{g}}\bigg[\tilde{g}^{\mu\nu}h^{\rho\kappa}h_\kappa^\sigma+\tilde{g}^{\rho\sigma}h^{\mu\kappa}h_\kappa^\nu-\frac{1}{2}\tilde{g}^{\mu\nu}hh^{\rho\sigma}-\frac{1}{2}\tilde{g}^{\rho\sigma}hh^{\mu\nu}+h^{\mu\nu}h^{\rho\sigma}
$$

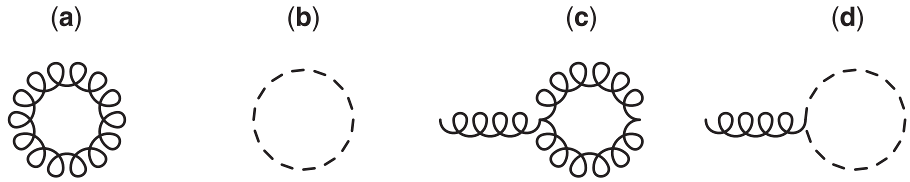

Fig. 6. Vacuum and tadpole diagrams.

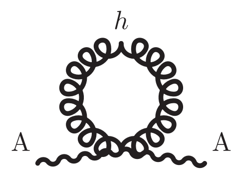

Fig. 7. Vector coupling renormalization.

$$+\frac{1}{8}\tilde{g}^{\mu\nu}\tilde{g}^{\rho\sigma}(h^2-2h_{\kappa_1\kappa_2}h^{\kappa_1\kappa_2})\Big]\tilde{F}_{\mu\rho}\tilde{F}_{\nu\sigma}. \tag{30}$$

The correlator to be computed is

$$-\frac{i}{4\mu^{2\epsilon}e^2}\int\sqrt{-\tilde{g}}\tilde{F}_{\mu\rho}\tilde{F}_{\nu\sigma}\Big\langle\tilde{g}^{\mu\nu}h^{\rho\kappa}h_{\kappa}^{\sigma}+\tilde{g}^{\rho\sigma}h^{\mu\kappa}h_{\kappa}^{\nu}-\frac{1}{2}\tilde{g}^{\mu\nu}hh^{\rho\sigma}-\frac{1}{2}\tilde{g}^{\rho\sigma}hh^{\mu\nu}$$
$$+h^{\mu\nu}h^{\rho\sigma}+\frac{1}{8}\tilde{g}^{\mu\nu}\tilde{g}^{\rho\sigma}(h^2-2h_{\kappa_1\kappa_2}h^{\kappa_1\kappa_2})\Big\rangle. \tag{31}$$

With the self-contractions of the fluctuation fields, the correlator leads to a counter-term of the form $\sim\tilde{F}^2_{\alpha\beta}$. Again, the result vanishes due to the identity in Eq. (64) in dimensional regularization. The shift can be introduced through finite renormalization. In Sect. 4 we revisit the renormalization of the coupling constants by employing an alternate renormalization scheme where the cosmological constant is treated as a formal graviton mass.

3. Flat space analysis

In this section we consider a flat background. The analysis can also be viewed as the computation of the divergences in a curved background: the flat space analysis captures them since the ultraviolet divergence is a short-distance phenomenon. In the past, the counter-terms were determined essentially by dimensional analysis and covariance [23].[6] We directly calculate them in the refined background field method; dimensional analysis and covariance play the *subsidiary* role of checking the results.

[6] Let us explain this point by taking the earlier work of Ref. [24], which makes it simpler to see the point, whose methodology was shared by Ref. [23]. In the beginning of Sect. 3 of [24], the authors considered a scalar system in a flat background. Their action (3.1) contains external fields; the 1PI effective action was worked out in the usual way. Note that the background fields, namely the external fields, are completely off-shell. Afterwards they considered a gravity case whose action is given in their (3.8). This time, however, the form of their action (3.9) was fixed based on the covariance and dimensional analysis. The coefficients of the counter-terms were then determined by considering certain Feynman diagrams with *on-shell* background fields and using the usual traceful propagator. As heavily stressed in our previous works [11,12], only the traceless propagator maintains the covariance. In the present work, the analogous calculation is performed with off-shell background fields, just as in the first example, i.e. the scalar case of Ref. [24].

Let us consider a flat background so that

$$\hat{g}_{\mu\nu} \equiv h_{\mu\nu} + \tilde{g}_{\mu\nu}, \qquad \hat{A}_\mu \equiv a_\mu + \tilde{A}_\mu, \tag{32}$$

where

$$\tilde{g}_{\mu\nu} \equiv \varphi_{\mu\nu} + g_{\mu\nu}, \qquad \tilde{A}_\mu \equiv A_\mu + A_{0\mu} \tag{33}$$

and now

$$g_{\mu\nu} = \eta_{\mu\nu}, \qquad A_{0\mu} = 0. \tag{34}$$

We employ dimensional regularization. In what follows we will present the explicit flat spacetime computations for the two-point diagrams considered for a generic background $g_{\mu\nu}$ in the previous section. Although the techniques of the counter-term computation themselves are similar to those used in the pure gravity [12] and gravity-scalar [15] analyses, the present case has several additional complications. As an unexpected spin-off of our direct approach, we will see how the newly noted gauge choice dependence issue is resolved in the present framework. In Sect. 3.2 we also address how the well-known gauge choice dependence may be avoided, especially for a de Donder-type gauge, for the physical states in the present framework.

3.1. *Two-point diagrams*

The pure gravity sector was analyzed in Ref. [12]. Consider the ghost loop diagram in Fig. 2(b) first. The ghost vertex takes, in the flat spacetime,

$$V_C = -\big[-\tilde{\Gamma}^\lambda_{\mu\nu}(-C_\lambda\partial^\mu\bar{C}^\nu + \bar{C}_\lambda\partial^\mu C^\nu) - (\eta^{\nu\beta}\varphi^{\mu\alpha} + \eta^{\mu\alpha}\varphi^{\nu\beta})\partial_\beta\bar{C}_\alpha\partial_\nu C_\mu\big] + R_{\mu\nu}\bar{C}^\mu C^\nu.$$

Let us define, for convenience, $V_C = V_{C,I} + V_{C,II}$ with

$$\begin{aligned} V_{C,I} &\equiv -\big[-\tilde{\Gamma}^\lambda_{\mu\nu}(-C_\lambda\partial^\mu\bar{C}^\nu + \bar{C}_\lambda\partial^\mu C^\nu) - (\eta^{\nu\beta}\varphi^{\mu\alpha} + \eta^{\mu\alpha}\varphi^{\nu\beta})\partial_\beta\bar{C}_\alpha\partial_\nu C_\mu\big],\\ V_{C,II} &\equiv R_{\mu\nu}\bar{C}^\mu C^\nu. \end{aligned} \tag{35}$$

The correlator to be computed is

$$\begin{aligned} -\frac{1}{2}\frac{1}{\kappa'^4}\left\langle\left(\int V_{C,I} + V_{C,II}\right)^2\right\rangle = -\frac{1}{2}\frac{1}{\kappa'^4}\Big\langle\Big\{\int\big[-\tilde{\Gamma}^\lambda_{\mu\nu}(\partial^\mu\bar{C}^\nu C_\lambda - \partial^\mu C^\nu\bar{C}_\lambda)\\ - (\eta^{\nu\beta}\varphi^{\mu\alpha} + \eta^{\mu\alpha}\varphi^{\nu\beta})\partial_\beta\bar{C}_\alpha\partial_\nu C_\mu\big] - R_{\mu\nu}\bar{C}^\mu C^\nu\Big\}^2\Big\rangle. \end{aligned} \tag{36}$$

To see how the dimensional analysis and covariance can be utilized to check the final results, consider, e.g., $\langle(\int V_{C,I})^2\rangle$; a direct calculation yields

$$\begin{aligned} -\frac{1}{2}\frac{1}{\kappa'^4}\left\langle\left(\int V_{C,I}\right)^2\right\rangle = \\ -\frac{1}{2}\frac{\Gamma(\varepsilon)}{(4\pi)^2}\int\left[-\frac{2}{15}\partial^2\varphi_{\mu\nu}\partial^2\varphi^{\mu\nu} + \frac{4}{15}\partial^2\varphi^{\alpha\kappa}\partial_\kappa\partial_\sigma\varphi^\sigma_\alpha - \frac{1}{30}(\partial_\alpha\partial_\beta\varphi^{\alpha\beta})^2\right], \end{aligned} \tag{37}$$

where the parameter ε is related to the total spacetime dimension D by

$$D = 4 - 2\varepsilon. \tag{38}$$

The result above (and some below) were obtained with the help of the Mathematica package xAct'xTensor' in performing the index contractions. By invoking dimensional analysis and covariance, one expects the result to come out to be a sum of R^2 and $R^2_{\mu\nu}$ to the second order of $\varphi_{\rho\sigma}$ with appropriate coefficients. With the traceless condition $\varphi = 0$ explicitly enforced, R^2 and $R^2_{\mu\nu}$ are given, to the second order in $\varphi_{\alpha\beta}$, by

$$\begin{aligned} R^2 &= \partial_\mu \partial_\nu \varphi^{\mu\nu}\, \partial_\rho \partial_\sigma \varphi^{\rho\sigma}, \\ R_{\alpha\beta} R^{\alpha\beta} &= \frac{1}{4}\big[\partial^2 \varphi^{\mu\nu}\, \partial^2 \varphi_{\mu\nu} - 2\partial^2 \varphi^{\alpha\kappa}\, \partial_\kappa \partial_\sigma \varphi_\alpha^\sigma + 2(\partial_\mu \partial_\nu \varphi^{\mu\nu})^2\big]; \end{aligned} \tag{39}$$

from these, it follows that

$$-\frac{1}{2}\frac{1}{\kappa'^4}\left\langle \left(\int V_{C,I}\right)^2 \right\rangle = -\frac{1}{2}\frac{\Gamma(\varepsilon)}{(4\pi)^2} \int \left[-\frac{8}{15}\tilde{R}_{\alpha\beta}\tilde{R}^{\alpha\beta} + \frac{7}{30}\tilde{R}^2 \right]. \tag{40}$$

The tildes on the fields in the counter-terms will be omitted from now on. Let us complete the other terms in Eq. (36); collecting all, one gets, for the ghost diagram,

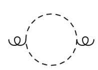

$$\Rightarrow -\frac{1}{2}\frac{\Gamma(\varepsilon)}{(4\pi)^2} \int \left[\frac{7}{15} R_{\mu\nu} R^{\mu\nu} + \frac{17}{30} R^2 \right]. \tag{41}$$

As for the graviton-loop diagram in Fig. 2(a), the vertex V_g takes

$$\begin{aligned} V_g \equiv{}& \big(2\eta^{\beta\beta'}\tilde{\Gamma}^{\alpha'\gamma\alpha} - \eta^{\alpha\beta}\tilde{\Gamma}^{\alpha'\gamma\beta'}\big)\partial_\gamma h_{\alpha\beta}\, h_{\alpha'\beta'} + \bigg[\frac{1}{2}\big(\eta^{\alpha\alpha'}\eta^{\beta\beta'}\varphi^{\gamma\gamma'} + \eta^{\beta\beta'}\eta^{\gamma\gamma'}\varphi^{\alpha\alpha'} \\ &+ \eta^{\alpha\alpha'}\eta^{\gamma\gamma'}\varphi^{\beta\beta'}\big) - \frac{1}{2}\eta^{\gamma\gamma'}\eta^{\alpha'\beta'}\varphi^{\alpha\beta} - \frac{1}{4}\varphi^{\gamma\gamma'}\eta^{\alpha\beta}\eta^{\alpha'\beta'}\bigg]\partial_\gamma h_{\alpha\beta}\, \partial_{\gamma'} h_{\alpha'\beta'} \\ &+ \left(h_{\alpha\beta} h_{\gamma\delta} \tilde{R}^{\alpha\gamma\beta\delta} - h_{\alpha\beta} h^\beta{}_\gamma \tilde{R}^{\kappa\alpha\gamma}{}_\kappa - \frac{1}{2} h^{\alpha\beta} h_{\alpha\beta}\tilde{R} \right). \end{aligned} \tag{42}$$

Let us define

$$\begin{aligned} V_{g,I} &\equiv \big(2\eta^{\beta\beta'}\tilde{\Gamma}^{\alpha'\gamma\alpha} - \eta^{\alpha\beta}\tilde{\Gamma}^{\alpha'\gamma\beta'}\big)\partial_\gamma h_{\alpha\beta}\, h_{\alpha'\beta'}, \\ V_{g,II} &\equiv \bigg[\frac{1}{2}(\eta^{\alpha\alpha'}\eta^{\beta\beta'}\varphi^{\gamma\gamma'} + \eta^{\beta\beta'}\eta^{\gamma\gamma'}\varphi^{\alpha\alpha'} + \eta^{\alpha\alpha'}\eta^{\gamma\gamma'}\varphi^{\beta\beta'}) \\ &\qquad - \frac{1}{4}\varphi\, \eta^{\alpha\alpha'}\eta^{\beta\beta'}\eta^{\gamma\gamma'} - \frac{1}{2}\eta^{\gamma\gamma'}\eta^{\alpha'\beta'}\varphi^{\alpha\beta} \\ &\qquad + \frac{1}{4}\left(-\varphi^{\gamma\gamma'} + \frac{1}{2}\varphi\eta^{\gamma\gamma'} \right)\eta^{\alpha\beta}\eta^{\alpha'\beta'}\bigg]\partial_\gamma h_{\alpha\beta}\, \partial_{\gamma'} h_{\alpha'\beta'}, \\ V_{g,III} &= \sqrt{-\tilde{g}}\left(h_{\alpha\beta} h_{\gamma\delta}\tilde{R}^{\alpha\gamma\beta\delta} - h_{\alpha\beta} h^\beta{}_\gamma \tilde{R}^{\kappa\alpha\gamma}{}_\kappa - \frac{1}{2} h^{\alpha\beta} h_{\alpha\beta}\tilde{R} \right). \end{aligned} \tag{43}$$

By using the traceless propagator one can show that

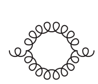

$$\Rightarrow -\frac{1}{2}\frac{\Gamma(\varepsilon)}{(4\pi)^2} \int \left[-\frac{23}{20} R_{\mu\nu} R^{\mu\nu} - \frac{23}{40} R^2 \right]. \tag{44}$$

The correlators for the matter-involving sector have also been outlined in the previous section. Their flat spacetime evaluation leads to the following results for the diagrams in Fig. 3(a)–(c):

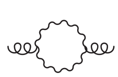

$$\Rightarrow \frac{\Gamma(\varepsilon)}{(4\pi)^2}\int\left(\frac{1}{30}R^2-\frac{1}{10}R_{\alpha\beta}R^{\alpha\beta}\right),$$

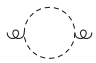

$$\Rightarrow -\frac{\Gamma(\varepsilon)}{(4\pi)^2}\frac{1}{15}\int R_{\alpha\beta}R^{\alpha\beta},$$

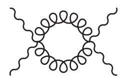

$$\Rightarrow \frac{\kappa'^4\,\Gamma(\varepsilon)}{(4\pi)^2}\frac{3}{64}\int (F_{\alpha\beta}F^{\alpha\beta})^2. \tag{45}$$

These results are covariant as expected. The direct calculation of the diagram in Fig. 3(d) yields

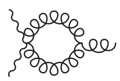

$$\Bigg|_{V_{g,I}+V_{g,II}} \Rightarrow \frac{\kappa'^2\,\Gamma(\varepsilon)}{(4\pi)^2}\int\left(\frac{1}{16}F_{\mu\nu}F^{\mu\nu}\partial_\alpha\partial_\beta\varphi^{\alpha\beta}+\frac{1}{2}F_{\mu\kappa}F_\nu{}^\kappa\partial^2\varphi^{\mu\nu}\right), \tag{46}$$

which is non-covariant.[7] As a matter of fact, this is the diagram that suggests the solution for the gauge choice dependence. This non-covariant result will be examined in Sect. 3.2, and we will see how the covariance is restored. The diagram above also receives a contribution from the $V_{g,III}$ vertex:

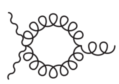

$$\Bigg|_{V_{g,III}} \Rightarrow \frac{\kappa'^2\,\Gamma(\varepsilon)}{(4\pi)^2}\int\bigg(\frac{3}{4}F_{\alpha\kappa}F_\beta{}^\kappa R^{\alpha\beta}+\frac{1}{8}F_{\alpha\beta}F^{\alpha\beta}R$$
$$+\frac{1}{4}F_{\alpha\delta}F_{\beta\gamma}R^{\alpha\beta\gamma\delta}-\frac{1}{4}F_{\alpha\beta}F_{\gamma\delta}R^{\alpha\beta\gamma\delta}\bigg). \tag{47}$$

As for the diagrams with the inhomogeneous loops, the first-layer diagram to be computed is the one in Fig. 5. It corresponds to several second-layer diagrams, two of which are Figs. 4(a) and (b); one can show that

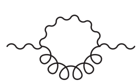

$$\Rightarrow \frac{\kappa'^2}{2}\frac{\Gamma(\varepsilon)}{(4\pi)^2}\int\left(\frac{1}{3}\partial_\alpha F^\alpha{}_\kappa\partial_\beta F^{\beta\kappa}-\frac{1}{12}\partial_\rho F_{\alpha\beta}\partial^\rho F^{\alpha\beta}\right),$$

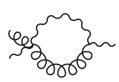

$$\Rightarrow \kappa'^2\frac{\Gamma(\varepsilon)}{(4\pi)^2}\int\left(\frac{1}{3}F_{\alpha\kappa}\partial_\lambda\partial^\beta F_\beta{}^\kappa\varphi^{\alpha\lambda}-\frac{1}{12}F_{\alpha\kappa}\partial^2F_\beta{}^\kappa\varphi^{\alpha\beta}\right), \tag{48}$$

where all of the index contractions are done with the flat metric. Whereas the first diagram is covariant at the leading order, the second diagram is not at its given order, the $\varphi_{\alpha\beta}$-linear order. There are also contributions arising from the higher-order internal propagators, and all of these three different contributions are required for the covariance since together they correspond to the single first-layer diagram in Fig. 5. Keeping track of the higher-order internal propagators obviously requires the full (or at least higher-order) propagator expression $\tilde{\Delta}$. Therefore, instead of separately computing the individual contributions, it will be more economical to compute them at one stroke. The calculation can be done by performing the following steps:

Let us consider

$$\mathbf{V}\equiv\frac{1}{2}\big[\tilde{g}^{\rho\sigma}h^{\mu\nu}+\tilde{g}^{\mu\nu}h^{\rho\sigma}\big]f_{\mu\rho}F_{\nu\sigma}, \tag{49}$$

[7] In the case of the Einstein-scalar system analyzed in Ref. [15], we obtained a covariant result for a similar diagram, 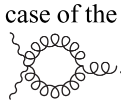. The present non-covariant result is one reflection of the complexity of the gauge matter system.

where the contractions are carried out by $\tilde{g}_{\mu\nu}$. At this point we introduce the orthonormal basis e_a^μ:

$$\tilde{e}_a^\mu \tilde{e}_b^\nu \tilde{g}_{\mu\nu} = \eta_{ab}, \tag{50}$$

where the Latin indices run over $a, b = 0, 1, 2, 3$. The full scalar propagator $\tilde{\Delta}$ can be written as

$$\tilde{\Delta}(X_1 - X_2) = \int \frac{d^4 L}{(2\pi)^4} \frac{e^{iL_c(X_1 - X_2)^c}}{iL_a L_b \eta^{ab}}, \tag{51}$$

where X^a and L_c are the coordinates and momenta associated with the orthonormal basis. Then, the computation of the two-point amplitude goes identically with that of Fig. 4(a); switching back to the original frame, one gets

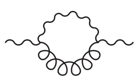

$$\Rightarrow -\frac{1}{2}\left\langle \left(\int \mathbf{V}\right)^2 \right\rangle = \frac{\kappa'^2}{2} \frac{\Gamma(\varepsilon)}{(4\pi)^2} \int \left(\frac{1}{3} \nabla_\alpha F^\alpha{}_\kappa \nabla_\beta F^{\beta\kappa} - \frac{1}{12} \nabla_\rho F_{\alpha\beta} \nabla^\rho F^{\alpha\beta} \right). \tag{52}$$

The analysis of the vacuum-to-vacuum amplitudes and tadpoles will be presented in Sect. 4.

3.2. On gauge choice and background independence

Above, we have evaluated the counter-terms for the diagrams in Figs. 2–6, and they have led to different types of counter-terms, one of which, i.e. Eq. (46), has come out non-covariant. This means that the effective action, as it stands, is non-covariant and gauge fixing dependent.[8] It turns out that these two problems have the following common solution: once the gauge fixing[9]

$$\partial_\mu \varphi^{\mu\nu} = 0 \tag{53}$$

is explicitly imposed on the effective action, the covariance and gauge choice independence are restored.

To see this, let us examine the non-covariant counter-terms for Fig. 3(c) given in Eq. (46). Note that the first term in Eq. (46) vanishes upon imposing the strong form of the gauge condition $\partial_\mu \varphi^{\mu\nu} = 0$, which implies[10]

$$\partial_\nu \partial_\mu \varphi^{\mu\nu} = 0; \tag{54}$$

with this, Eq. (46) now takes

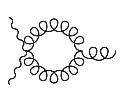

$$\Big|_{V_{g,I} + V_{g,II}} \Rightarrow \frac{\kappa'^2\, \Gamma(\varepsilon)}{(4\pi)^2} \int \left(\frac{1}{2} F_{\mu\kappa} F_\nu{}^\kappa \partial^2 \varphi^{\mu\nu} \right) = -\frac{\kappa'^2\, \Gamma(\epsilon)}{(4\pi)^2} \int F_{\mu\kappa} F_\nu{}^\kappa R^{\mu\nu}, \tag{55}$$

---

[8] In the intensive work of Ref. [33] (see also Refs. [31,32]), a certain gauge choice dependence was found even though Vilkovisky's method [37] was employed. (A similar related observation was made in Refs. [35,36].) The gauge choice dependence newly found in the present framework should have the same origin as that of Ref. [33] (see below) but be a different manifestation. The gauge choice dependence in the present work occurs through breaking of the covariance. It is milder and is easily fixable, as we will see. The well-known gauge choice dependence, which is addressed at the end of this subsection, is that the coefficients of the covariant terms in the 1PI effective action depend, in general, on one's chosen gauge (see, e.g., Refs. [34–36]). Whereas this type of gauge dependence occurs in a Yang–Mills theory as well, the present gauge dependence is unique to a gravity theory.

[9] Note that the gauge fixing $\partial_\mu \varphi^{\mu\nu} - \partial^\nu \varphi = 0$ reduces to Eq. (53) once the traceless condition $\varphi = 0$ is enforced.

[10] We have the following caveat. Since the scalar curvature R is given by $R = \partial_\alpha \partial_\beta \varphi^{\alpha\beta}$ to the linear order, it is not possible, with the strong form of the gauge condition, to probe the presence of the R-factor through the current linear-order calculation. For that, it is necessary to go to the second order.

where the second equality is valid, as usual, up to a certain order of $\varphi_{\alpha\beta}$, the linear order for the present case. Note that above, the following identity at $\varphi_{\rho\sigma}$-linear order has been used:

$$R_{\mu\nu} = \frac{1}{2}\left(\partial^\kappa \partial_\mu \varphi_{\kappa\nu} + \partial^\kappa \partial_\nu \varphi_{\kappa\mu} - \partial_\mu \partial_\nu \varphi - \partial^2 \varphi_{\mu\nu}\right) = -\frac{1}{2}\partial^2 \varphi_{\mu\nu}, \tag{56}$$

where the second equality results once the gauge conditions are enforced.

The effective action becomes fully covariant and gauge choice independent after enforcing $\partial_\nu \varphi^{\mu\nu} = 0$. In this sense, the novel gauge choice dependence found in the present work is mild, due to the use of the traceless propagator and refined background field method. Also, among the terms explicitly evaluated above, only Eq. (46) has the issue; all the other terms are gauge fixing independent. In particular, the F^2 is gauge choice independent, although we did not record the result (since our focus is the cosmological and Newton constants), a result consistent with Refs. [39,40].

One should view the covariant action as still supplemented by the gauge fixing. (This is just like the classical action, which is fully covariant but is to be supplemented by a gauge-fixing condition.) If one chooses a different gauge fixing and carries out the amplitude computations in that gauge, one should get exactly the same covariant effective action up to the terms that can be removed by that gauge condition; this time, the action is supplemented with the very gauge-fixing condition that one has chosen. Therefore, the gauge choice independence of the effective action should be interpreted to mean that the action is covariant after enforcing the strong form of the gauge condition, and that the covariant action is to be supplemented by one's chosen gauge-fixing condition. (But, one can of course choose any gauge fixing (even a gauge fixing different from the initial one) once the covariant effective action is obtained.)

One may wonder whether the appearance of the factors of $\partial_\mu \varphi^{\mu\nu}$ in the counter-term calculation of Eq. (46) could by any chance be made to disappear, say, without imposing the gauge condition. It appears that the gauge choice dependence has a deeper root. To be specific, let us consider the proof of the gauge choice independence in Chapter 15 of Ref. [46]. The proof is for a gauge theory in the ordinary (i.e. non-BFM) path integral. The gauge choice dependence gets to reside in a field-independent constant (denoted there by C; see their Eq. (15.5.19)), which is then duly disregarded. If one employs the BFM, however, that constant comes to depend on the background fields (say, $\varphi_{\mu\nu}$ for the present case, for example), and this must be the gauge choice dependence that we have observed. This shows that the BFM, refined or not, has a limitation when applied to a gravitational system: it is introduced aiming for a more covariant treatment of the effective action computation, but turns out to be at odds with the gauge choice independence.[11] The limitation is overcome by imposing the gauge condition in its strong form, as we have just discussed.

Finally, let us address the well-known long-standing gauge choice dependence followed by background (in)dependence. This long-noted gauge choice dependence of the effective action had been studied in a number of papers in the past, including Refs. [31–41]. In Refs. [35,36], in particular, it was shown to disappear on-shell. We examine two aspects of the issue. The first is most relevant for the effective action computation and beta function computation in Sect. 4.3. The second concerns the gauge choice independence of scattering amplitudes, i.e. the gauge choice independence of the S-matrix.

[11] Nevertheless, the refined BFM has an advantage compared to the conventional BFM in that the latter would yield results non-covariant in an uncontrollable way whereas the former gives the results covariant up to the gauge-choice-dependent terms that can be removed by enforcing the strong form of the gauge condition.

For the first aspect, let us recall that one specific way of posing the potential gauge choice dependence issue is to consider the following type of gauge-fixing term,

$$-\frac{1}{2\xi}\Big[\tilde{\nabla}_\nu h^{\mu\nu} - \frac{\rho}{2}\tilde{\nabla}^\mu h\Big]^2, \tag{57}$$

and ask whether or not the constants ξ, ρ appear in the effective action. Since the propagator is traceless, the trace term h can simply be omitted, as commented earlier. This ensures the ρ independence of the computation. As for the constant ξ, see the comments below Eq. (61).

The second aspect will be most relevant for the gauge choice independence of the S-matrix. The upshot is that the dependence may be avoided for the "physical states." The present framework is in line with Refs. [35,36], and refines it in the sense that only a part of the field equations should be required. To see this, let us recall the physical states are defined as a solution of the Hamiltonian and momentum constraints in the Arnowitt–Deser–Misner (ADM) formalism; see, e.g., Ref. [10] for more details. The full nonlinear form of the de Donder gauge is given by

$$\hat{g}^{\rho\sigma}\hat{\Gamma}^\mu_{\rho\sigma} = 0, \tag{58}$$

where $\hat{g}^{\rho\sigma}$ denotes a generic metric and $\hat{\Gamma}^\mu_{\rho\sigma}$ the Christoffel symbols. In the ADM formalism the condition in Eq. (58) splits into

$$\begin{aligned}(\partial_{x^3} - \hat{N}^m\partial_m)\hat{n} &= \hat{n}^2\hat{K},\\ (\partial_{x^3} - \hat{N}^n\partial_n)\hat{N}^m &= \hat{n}^2(\hat{\gamma}^{mn}\partial_n \ln \hat{n} - \hat{\gamma}^{pq}\hat{\Gamma}^m_{pq}),\end{aligned} \tag{59}$$

where $\hat{n}$ and $\hat{N}^m$ are the lapse function and shift vector, $\hat{K}$ denotes the trace of the second fundamental form, and $\hat{\gamma}^{pq}$ is the 3D metric. Let us demonstrate the point for the fluctuations in a flat background; the conclusion will remain valid for a curved background. The physical states are defined as a solution of the Hamiltonian and momentum constraints. Since $\hat{n}$ and $\hat{N}^m$ are non-dynamical, they can be gauged away. (See Ref. [10] for a review.) With this, the first equation of Eq. (59) is satisfied, and the second becomes

$$\hat{\gamma}^{pq}\hat{\Gamma}^m_{pq} = 0, \tag{60}$$

which is nothing but the gauge-fixing condition adopted for the 3D analysis [11]. This suggests, in light of the discussion above on the origin of the dependence, that the amplitude will be independent of the non-physical states, i.e. will be gauge fixing independent, once the external states are restricted to the physical states. Recall now that the Hamiltonian and momentum constraints are nothing but the field equations of the lapse and shift in the Lagrangian formalism [11]. In other words, they are partially on-shell (but do not have to be fully on-shell). More specifically, let us consider a scattering amplitude

$$\langle \text{out}; \{\beta\} | \text{in}; \{\alpha\}\rangle, \tag{61}$$

where $|\text{in}; \{\alpha\}\rangle$ and $|\text{out}; \{\beta\}\rangle$ denote in and out states, respectively; $\{\alpha\}$ and $\{\beta\}$ collectively stand for various quantum numbers, such as angular momentum, spin, etc., carried by the Fock oscillators. Since the metric field is not a gauge singlet, such an amplitude, not being gauge invariant, will be generally gauge choice dependent. By definition, the physical states are inert under the bulk gauge transformation: once the external states are taken to be the physical states,[12] the amplitude will be gauge invariant and thus independent of gauge redundancy. Similarly, as for the potential ξ dependence of the effective action, it is expected that the effective action will, in general, depend on ξ. This is because the effective action corresponds to the amplitude in Eq. (61), with only the 1PI diagrams collected, with both in and out states taken as the 4D vacuum, and the 4D vacuum is not the physical vacuum. Once the in and out states are taken as the physical vacuum, the resulting effective action should be independent of gauge redundancy. However, a subtle possibility is that the 3D de Donder gauge in Eq. (60) may also contain, when considered in the context of a large gauge transformation, a labeling of different sectors of the physical degrees of freedom. (The reason for this expectation is as follows. In Ref. [47] it was shown that the residual symmetry of the de Donder gauge imposes a constraint on the gauge parameter. It is unlikely that the parameters of the large gauge transformation will satisfy it.) If that is the case, which seems to be a reasonable possibility, even the reduced action (see footnote 12) will depend on ξ, but the interpretation would be different: the dependence should be viewed as analogous to dependence of an amplitude on a global symmetry.

As for the background independence, the use of the full propagator greatly reduces the amount of computation, as we have seen in Eq. (52). Combined with freedom in choosing renormalization conditions, the use of the first-layer or "one-stroke" propagator may also have far-reaching consequences in implementing background-independent analysis. It is evident that computations carried out with the full propagator of Eq. (51) will yield background-independent results. The background dependence is implicit in the transformation associated with Eq. (50). As for the infrared sector contribution, at the end it may well be that the ever-powerful freedom in the renormalization conditions can be chosen to reflect the characteristics of the actual background.

4. One-loop renormalization

The focus of the previous section was on the divergent parts of the diagrams; the analysis was involved but relatively straightforward. The forms of the counter-terms have been obtained, with the infinite parts of the coefficients specified. As is well known in standard quantum field theory, one has the freedom to adjust the finite parts of the coefficients through the renormalization scheme, which one may take to be the modified minimal subtraction $\overline{\mathrm{MS}}$ (see, e.g., Ref. [48] for a review). The main focus of the present section is to carry out the renormalization in detail and study its implications.

For the detailed analysis involving the renormalization conditions, it is convenient, as is commonly done, to introduce a scale parameter μ by making the following scaling:

$$\kappa^2 \to \mu^{-D+4}\kappa^2, \tag{62}$$

With this, Eq. (1) takes

$$S = \int \sqrt{-\hat{g}}\left(\frac{1}{\kappa^2\mu^{4-D}}\hat{R} - \frac{1}{4}\hat{F}^2_{\mu\nu}\right). \tag{63}$$

One can proceed and compute various amplitudes and counter-terms; that was basically what we did in the previous section, but this time the parameter μ will be included. The finite parts can now be kept track of with the fixed renormalization scheme.

[12] At the action level, taking the physical vacuum states corresponds to carrying out a certain dimensional reduction whose explicit procedure can be found in Ref. [47] for pure gravity. The reduction process is, of course, what makes the action partially on-shell [10], as mentioned above Eq. (61).

One of the main goals of this section is to analyze the renormalization of the cosmological and Newton constants (earlier works are, e.g., Refs. [35,36,49,50]). In its entirety the procedure involves dealing with an infinite number of counter-terms, not just the cosmological constant and Einstein–Hilbert terms. It will nevertheless be useful to first hone in on the renormalization of those two constants, a task undertaken at the end of Sect. 4.1, before working out the further details of the whole procedure in Sect. 4.2. This is because these constants carry special physical meanings, unlike the other newly appearing couplings that will ultimately be absorbed by a metric field redefinition. Moreover, there are some subtleties in the evaluation of the diagrams responsible for their renormalization.

Let us first frame the analysis of the vacuum and tadpole diagrams in preparation for Sect. 4.1. The vacuum-to-vacuum amplitude in Fig. 6(a) takes the form of the cosmological constant term and diverges (see, e.g., Refs. [15,46]). (The discussion here is for a flat spacetime, but the divergence will be quite generically produced for an arbitrary background.) Thus, if we were dealing with a massive theory it would take a counter-term of the form of the cosmological constant with infinite value to remove the divergence. However, the vacuum energy diagram vanishes due to an identity in dimensional regularization; see Eq. (68). This is a rather undesirable feature of dimensional regularization when dealing with a massless theory.[13] The diagrams responsible for the renormalization of Newton's constant are the tadpole diagrams. As we will see in detail in Sect. 4.1, the (would-be) shift in Newton's constant is caused by a diagram that results from the self-contraction of two fluctuation fields within the given vertex. Again, the following identity makes the regularization less suitable for the tadpole diagrams:

$$\int d^D k \frac{1}{(k^2)^\omega} = 0, \tag{64}$$

where ω is an arbitrary number. The tadpole diagram vanishes due to this: the divergence that would otherwise renormalize Newton's constant is taken to vanish. For reasons to be explained, we will introduce the shifts in the cosmological and Newton constants through finite renormalization.

4.1. Vacuum-to-vacuum and tadpole diagrams

The kinetic terms are responsible for the vacuum-to-vacuum amplitudes in the parlance of the first-layer perturbation. We quote them here for convenience:

$$\begin{aligned} 2\kappa^2 \mathcal{L} &= \sqrt{-\tilde{g}} \left(-\frac{1}{2} \tilde{\nabla}_\gamma h^{\alpha\beta} \tilde{\nabla}^\gamma h_{\alpha\beta} + \frac{1}{4} \tilde{\nabla}_\gamma h^\alpha_\alpha \tilde{\nabla}^\gamma h^\beta_\beta \right) \\ &= -\frac{1}{2} \partial_\gamma h^{\alpha\beta} \partial^\gamma h_{\alpha\beta} + \frac{1}{4} \partial_\gamma h^\alpha_\alpha \partial^\gamma h^\beta_\beta + V_{g,I} + V_{g,II}, \end{aligned} \tag{65}$$

[13] For instance, the identities in Eqs. (64) and (68) often obscure cancellations between the bosonic and fermionic amplitudes in a supersymmetric field theory, making them separately vanish.

where

$$\begin{aligned} V_{g,I} &\equiv \left(2\eta^{\beta\beta'}\tilde{\Gamma}^{\alpha'\gamma\alpha} - \eta^{\alpha\beta}\tilde{\Gamma}^{\alpha'\gamma\beta'}\right)\partial_\gamma h_{\alpha\beta}\, h_{\alpha'\beta'}, \\ V_{g,II} &\equiv \Bigg[\frac{1}{2}\left(\eta^{\alpha\alpha'}\eta^{\beta\beta'}\varphi^{\gamma\gamma'} + \eta^{\beta\beta'}\eta^{\gamma\gamma'}\varphi^{\alpha\alpha'} + \eta^{\alpha\alpha'}\eta^{\gamma\gamma'}\varphi^{\beta\beta'}\right) \\ &\quad - \frac{1}{4}\varphi\,\eta^{\alpha\alpha'}\eta^{\beta\beta'}\eta^{\gamma\gamma'} - \frac{1}{2}\eta^{\gamma\gamma'}\eta^{\alpha'\beta'}\varphi^{\alpha\beta} \\ &\quad + \frac{1}{4}\left(-\varphi^{\gamma\gamma'} + \frac{1}{2}\varphi\eta^{\gamma\gamma'}\right)\eta^{\alpha\beta}\eta^{\alpha'\beta'}\Bigg]\partial_\gamma h_{\alpha\beta}\,\partial_{\gamma'}h_{\alpha'\beta'}, \\ V_{g,III} &= \sqrt{-\tilde{g}}\left(h_{\alpha\beta}h_{\gamma\delta}\tilde{R}^{\alpha\gamma\beta\delta} - h_{\alpha\beta}h^{\beta}{}_{\gamma}\tilde{R}^{\kappa\alpha\gamma}{}_{\kappa} - \frac{1}{2}h^{\alpha\beta}h_{\alpha\beta}\tilde{R}\right). \end{aligned} \tag{66}$$

The vacuum-to-vacuum amplitudes in the first-layer perturbation can be split into two parts in the second-layer perturbation: the vacuum-to-vacuum amplitudes and the tadpoles.[14] Let us consider the vacuum-to-vacuum amplitudes in the second-layer perturbation. The vacuum energy, which leads to the cosmological constant renormalization, comes from

$$\int \prod_x dh_{\kappa_1\kappa_2}\ \exp\left\{\frac{i}{\kappa'^2}\int\ \left(-\frac{1}{2}\partial_\gamma h^{\alpha\beta}\partial^\gamma h_{\alpha\beta}\right)\right\}. \tag{67}$$

One obtains a constant term (see, e.g., the analysis given in Ref. [46]) whose divergent part (which will be denoted by A_0 in Eq. (70)[15]) is essentially the coefficient of the cosmological constant term. The calculation above leads to a quantum-level cosmological constant. Here is the difference between gravity and a non-gravitational theory. In a non-gravitational theory, the appearance of a term absent in the classical action would potentially be a signal toward non-renormalizability.[16] However, in a gravitational theory one has the additional leverage of a metric field redefinition, and we will ponder in Sect. 4.2 the significance of the quantum shift in the cosmological constant in the quantization framework that involves the metric field redefinition.

The evaluation of the vacuum-to-vacuum amplitude, whether it is from the graviton or the ghost (or matter), involves the following integral that is taken to vanish in dimensional regularization:

$$\int d^4p \ln p^2 = 0. \tag{68}$$

Nevertheless, we introduce renormalization by finite renormalization for the following reasons. Although the expression above is taken to vanish in dimensional regularization, the vacuum energy expression (in particular A_0 in Eq. (70)) will not, in general, vanish in other regularization methods for a curved background. To better examine the behavior of the integral, let us add a mass term m^2 that will be taken to $m^2 \to 0$ at the end:

$$\sim \int d^4p \ln\left(p^2 + m^2\right). \tag{69}$$

[14] As we will soon see, there are genuine tadpoles as well, i.e. tadpoles in the first-layer perturbation. As usual, we evaluate them through the second-layer perturbation.

[15] Note that $A_0 = -\mathscr{I}_{\text{div}}$ is used, e.g., in Ref. [15].

[16] Even in a non-gravitational theory, appearance of a *finite* number of new couplings is taken to be compatible with renormalizability.

One can then take derivatives with respect to m^2 for its evaluation; the result takes the form

$$A_{\rm f} + A_0 + A_1 m^2 + A_2 m^4, \tag{70}$$

where the A are some m-independent constants; the finite piece, $A_{\rm f}$, takes

$$A_{\rm f} \sim m^4 \ln m^2. \tag{71}$$

With the limit $m^2 \to 0$, only the term with the constant A_0, which is infinite, survives, and in dimensional regularization one sets $A_0 = 0$. Although each term in Eq. (70) either vanishes or is taken to zero, not introducing non-vanishing finite pieces seems unnatural (and is unlikely to be consistent with experiment); in a more general procedure of renormalization of a quantum field theory, one can always conduct finite renormalization regardless of the presence of the divergences. (As we will see in Sect. 4.2, not only does the quantum shift need to be introduced, but also the "classical" piece of the cosmological constant.) Once a finite piece is introduced and the definition of the physical cosmological constant is made (say, as the coefficient of the $\int \sqrt{-\tilde{g}}$ term), the renormalized coupling will run basically due to the presence of the scale parameter μ.

Let us now consider the tadpole diagrams, which[17] are responsible for the renormalization of Newton's constant. For the tadpole, the rest of vertices in the kinetic term in Eq. (65), which are nothing but $V_{g,I}$ and $V_{g,II}$, as well as $V_{g,III}$, are relevant; the former are part of the vacuum-to-vacuum amplitude in the first-layer perturbation, whereas the latter is associated with a genuine tadpole of the first-layer perturbation. It turns out that $V_{g,I}$ and $V_{g,II}$ lead to vanishing results in dimensional regularization; we illustrate that with $V_{g,I}$:

$$V_{g,I} = \left(2\eta^{\beta\beta'}\tilde{\Gamma}^{\alpha'\gamma\alpha} - \eta^{\alpha\beta}\tilde{\Gamma}^{\alpha'\gamma\beta'}\right)\partial_\gamma h_{\alpha\beta}\, h_{\alpha'\beta'}. \tag{72}$$

The self-contraction of the $h_{\mu\nu}$ in Eq. (72) leads to a momentum loop integral with an odd integrand, which thus vanishes. (The other terms in Eq. (65) vanish because the self-contraction leads to the trace of $\varphi_{\mu\nu}$.) The vertex $V_{g,III}$ similarly leads to a vanishing result. To see this, consider contraction of the $h_{\alpha\beta}$ fields in $V_{g,III}$. The index structures yield R, but the self-contraction is taken to vanish in dimensional regularization due to the identity in Eq. (64). Then, for the renormalization of Newton's constant the story goes similarly to the case of the cosmological constant: although the dimensional regularization does not lead to a divergence for the tadpole diagram, the shift is introduced through finite renormalization.

4.2. Renormalization by field redefinition

The full one-loop renormalization procedure is in order. Many steps of the procedure below have analogous steps in the Einstein-scalar case studied in Refs. [15,18]. Here, we put more effort into keeping track of the finite parts, and comparison with the future experimental results is elucidated in more detail.

[17] Typically, tadpole diagrams in a non-gravitational theory are cancelled by a counter-term linear in the field and not considered further. More care is needed in a gravitational theory since the counter-terms take the form of the Einstein–Hilbert term. At least a priori it seems safer to view its effect as shifting Newton's constant. The shift can be set to zero later if, for instance, the consistency of the renormalization program demands its vanishing.

Combining all the results so far, the renormalized action plus the counter-terms are given by

$$\int \sqrt{-g}\ (e_1 + e_2 R + e_3 R^2 + e_4 R^2_{\alpha\beta})$$
$$+ \int \sqrt{-g}\big(e_5 F_{\mu\kappa} F_\nu{}^\kappa R^{\mu\nu} + e_6 F_{\alpha\beta} F^{\alpha\beta} R + e_7 F_{\alpha\delta} F_{\beta\gamma} R^{\alpha\beta\gamma\delta}$$
$$+ e_8 F_{\alpha\beta} F_{\gamma\delta} R^{\alpha\beta\gamma\delta} + e_9 \nabla^\alpha F_{\alpha\kappa} \nabla^\beta F_\beta{}^\kappa + e_{10} \nabla_\lambda F_{\mu\nu} \nabla^\lambda F^{\mu\nu} + e_{11} (F_{\alpha\beta} F^{\alpha\beta})^2 + \cdots\big), \quad (73)$$

where e_1 is the constant previously denoted by A_0. More precisely, $[e_1] = A_0$, where the square bracket $[e_i]$ denotes the infinite parts of the coefficient e_i calculated by employing dimensional regularization. Similarly, the would-be divergence of the tadpole diagrams will be denoted $B_0 = [e_2]$. (A_0 and B_0 are taken to vanish in dimensional regularization.) For the rest of the coefficients, one has, by collecting the results in Sect. 3,

$$[e_3] = -\frac{17}{60} + \frac{23}{80} + \frac{1}{30}, \qquad [e_4] = -\frac{7}{30} + \frac{23}{40} - \frac{1}{10} - \frac{1}{15},$$
$$[e_5] = \Big(-1 + \frac{3}{4}\Big)\kappa'^2, \quad [e_6] = \frac{\kappa'^2}{8}, \quad [e_7] = \frac{\kappa'^2}{4}, \quad [e_8] = -\frac{\kappa'^2}{4},$$
$$[e_9] = \frac{\kappa'^2}{6}, \quad [e_{10}] = -\frac{\kappa'^2}{24}, \quad [e_{11}] = \frac{3}{64}\kappa'^4, \quad (74)$$

where the common factor $\frac{\Gamma(\varepsilon)}{(4\pi)^2}$ has been suppressed. The finite pieces of each coefficient are determined by the $\overline{\text{MS}}$ scheme. Not all these counter-terms are independent because of the following relationships, the second of which is valid up to total derivative terms:

$$F_{\alpha\beta} F_{\gamma\delta} R^{\alpha\beta\gamma\delta} = \nabla_\mu F_{\nu\rho} \nabla^\mu F^{\nu\rho} + 2 F_{\mu\kappa} F_\nu{}^\kappa R^{\mu\nu} - 2 \nabla^\lambda F_{\lambda\kappa} \nabla^\sigma F_\sigma{}^\kappa,$$
$$F_{\alpha\delta} F_{\beta\gamma} R^{\alpha\beta\gamma\delta} = -\frac{1}{2} F_{\alpha\beta} F_{\gamma\delta} R^{\alpha\beta\gamma\delta}. \quad (75)$$

Upon substituting these into Eq. (73), one gets[18]

$$\int \sqrt{-g}\big[e_1 + e_2 R + e_3 R^2 + e_4 R^2_{\alpha\beta} + (e_5 - e_7 + 2e_8) F_{\mu\kappa} F_\nu{}^\kappa R^{\mu\nu}$$
$$+ e_6 F_{\alpha\beta} F^{\alpha\beta} R + (e_7 - 2e_8 + e_9) \nabla^\alpha F_{\alpha\kappa} \nabla^\beta F_\beta{}^\kappa$$
$$+ (-e_7/2 + e_8 + e_{10}) \nabla_\lambda F_{\mu\nu} \nabla^\lambda F^{\mu\nu} + e_{11} (F_{\alpha\beta} F^{\alpha\beta})^2 + \cdots\big]. \quad (76)$$

The strategy is to absorb these counter-terms by redefining the metric in the bare action. Inspection reveals that the counter-terms of the forms $\nabla_\lambda F_{\mu\nu} \nabla^\lambda F^{\mu\nu}$ and $\nabla^\alpha F_{\alpha\kappa} \nabla^\beta F_\beta{}^\kappa$ cannot be absorbed by a bare action that consists of the Einstein–Hilbert term and the Maxwell term: one needs the cosmological constant term as well. The reason is that under a metric shift $g_{\mu\nu} \to g_{\mu\nu} + \delta g_{\mu\nu}$, the Einstein–Hilbert part shifts according to

$$\sqrt{-g}\, R \to \sqrt{-g}\, R + R\, \delta g^{\mu\nu} \frac{\delta\sqrt{-g}}{\delta g_{\mu\nu}} + \sqrt{-g}\, \delta g^{\mu\nu} \frac{\delta R}{\delta g_{\mu\nu}}, \quad (77)$$

[18] The analysis in this section is to illustrate the renormalization procedure and is based on the computation that we have carried out in the previous sections. Some of the diagrams that we did not explicitly calculate will change the numerical values of certain coefficients.

so the shifted part comes either with R or $R_{\mu\nu}$, and is thus inadequate to absorb the aforementioned counter-terms; so is the shifted part from the Maxwell action. We assume the presence of the cosmological constant in the bare action and proceed; more in the conclusion.

Let us consider the following shifts [15,51]:[19]

$$\begin{aligned}
&\kappa \to \kappa + \delta\kappa, \\
&\Lambda \to \Lambda + \delta\Lambda, \\
&g_{\mu\nu} \to \mathscr{G}_{\mu\nu} \equiv l_0 g_{\mu\nu} + l_1 g_{\mu\nu} R + l_2 R_{\mu\nu} + l_3 g_{\mu\nu} F^2_{\rho\sigma} + l_4 F_{\mu\kappa} F_\nu{}^\kappa \\
&\qquad + l_5 R F_{\mu\kappa} F_\nu{}^\kappa + l_6 R_{\mu\nu} F^2_{\kappa_1\kappa_2} + l_7 g_{\mu\nu} R F^2_{\rho\sigma} + l_8 g_{\mu\nu} R^{\alpha\beta} F_{\alpha\kappa} F_\beta{}^\kappa \\
&\qquad + l_9 R_\mu{}^\alpha{}_\nu{}^\beta F_{\alpha\kappa} F_\beta{}^\kappa + l_{10} R (F_{\kappa_1\kappa_2} F^{\kappa_1\kappa_2})^2 \\
&\qquad + l_{11} \nabla_\mu F_{\kappa_1\kappa_2} \nabla_\nu F^{\kappa_1\kappa_2} + l_{12} \nabla^\lambda F_{\lambda\mu} \nabla^\kappa F_{\kappa\nu}.
\end{aligned} \tag{78}$$

One can straightforwardly show that under these, the gravity and matter sectors shift, respectively, by

$$\begin{aligned}
&-\left(\frac{2}{\kappa^2}\Lambda\right) \int \sqrt{-g} + \frac{1}{\kappa^2} \int d^4x \sqrt{-g}\, R \to -2\left(\frac{\Lambda}{\kappa^2} + \frac{\delta\Lambda}{\kappa^2} - \frac{2\delta\kappa\,\Lambda}{\kappa^3} + 2l_0\Lambda\right) \int \sqrt{-g} \\
&\quad + \left(\frac{1}{\kappa^2} - \frac{2\delta\kappa}{\kappa^3} + \frac{l_0}{\kappa^2} - \frac{\Lambda}{\kappa^2}(4l_1 + l_2)\right) \int \sqrt{-g}\, R + \frac{1}{\kappa^2} \int \sqrt{-g}\left[\left(l_1 + \frac{1}{2}l_2\right) R^2 - l_2 R_{\mu\nu} R^{\mu\nu}\right] \\
&\quad + \frac{1}{\kappa^2} \int \sqrt{-g}\Big[-\Lambda(4l_3 + l_4) F_{\alpha\beta} F^{\alpha\beta} + \Big(l_3 + l_4/2 - \Lambda[l_5 + l_6 + 4l_7]\Big) R F_{\alpha\beta} F^{\alpha\beta} \\
&\quad - \Lambda(4l_8 + l_9) R^{\alpha\beta} F_{\alpha\kappa} F_\beta{}^\kappa - 4\Lambda l_{10} (F_{\rho\sigma} F^{\rho\sigma})^2 - \Lambda l_{11} (\nabla_\mu F_{\nu\rho})^2 - \Lambda l_{12} (\nabla^\kappa F_{\kappa\nu})^2 + \ldots \Big]
\end{aligned} \tag{79}$$

and[20]

$$\begin{aligned}
-\frac{1}{4} \int \sqrt{-g}\, F^2_{\mu\nu} \to -\frac{1}{4} \int \sqrt{-g}\, F^2_{\mu\nu} + \int \sqrt{-g}\, \Big[&-\frac{l_2}{8} R F_{\alpha\beta} F^{\alpha\beta} \\
&+ \frac{l_2}{2} R^{\alpha\beta} F_{\alpha\kappa} F_\beta{}^\kappa + \frac{l_3}{2} (F_{\rho\sigma} F^{\rho\sigma})^2 + \frac{l_4}{2} F_{\alpha\kappa} F_\beta{}^\kappa F^{\alpha\kappa'} F^\beta{}_{\kappa'} + \cdots \Big].
\end{aligned} \tag{80}$$

Combining these two, one gets

$$\begin{aligned}
&\frac{1}{\kappa^2} \int d^4x \sqrt{-g}\, (R - 2\Lambda) - \frac{1}{4} \int \sqrt{-g}\, F^2_{\mu\nu} \to -2\left(\frac{\Lambda}{\kappa^2} + \frac{\delta\Lambda}{\kappa^2} - \frac{2\delta\kappa\,\Lambda}{\kappa^3} + 2l_0\Lambda\right) \int \sqrt{-g} \\
&\qquad + \left(\frac{1}{\kappa^2} - \frac{2\delta\kappa}{\kappa^3} + \frac{1}{\kappa^2} l_0 - \frac{1}{\kappa^2}\Lambda(4l_1 + l_2)\right) \int \sqrt{-g}\, R - \frac{1}{4} \int \sqrt{-g}\, F^2_{\mu\nu} \\
&\quad + \frac{1}{\kappa^2} \int \sqrt{-g}\left[\left(l_1 + \frac{1}{2}l_2\right) R^2 - l_2 R_{\mu\nu} R^{\mu\nu}\right] + \frac{1}{\kappa^2} \int \sqrt{-g}\Big[-\Lambda(4l_3 + l_4) F_{\alpha\beta} F^{\alpha\beta} \\
&\quad + \left(l_3 + \frac{l_4}{2} - \Lambda[l_5 + l_6 + 4l_7] - \frac{l_2}{8}\kappa^2\right) R F_{\alpha\beta} F^{\alpha\beta} + \left(\kappa^2 \frac{l_2}{2} - \Lambda[4l_8 + l_9]\right) R^{\alpha\beta} F_{\alpha\kappa} F_\beta{}^\kappa
\end{aligned}$$

---

[19] One may wonder about the traceless condition on the newly defined metric. The traceless condition was in order for the propagator to be well defined. Once the effective action is obtained, one may choose a different gauge fixing for solving the field equations in which the traceless condition may not be imposed.

[20] It is likely that the counter-term of the form $F_{\alpha\kappa} F_\beta{}^\kappa F^{\alpha\kappa'} F^\beta{}_{\kappa'}$ will appear at the two-loop level.

$$(\kappa^2 l_3/2 - 4\Lambda l_{10})(F_{\rho\sigma}F^{\rho\sigma})^2 - l_{11}(\nabla_\mu F_{\nu\rho})^2 - l_{12}(\nabla^\kappa F_{\kappa\nu})^2 + \cdots \Big]. \tag{81}$$

Not all of the terms in the expansion have been explicitly recorded: additional diagrams such as three-point amplitudes should be considered to account for some of them.

Let us consider the first several coefficients of the shifted action and compare them with those of Eq. (76). We start with the cosmological constant term and the Einstein–Hilbert term. Their counter-terms can be absorbed by setting

$$-\frac{2}{\kappa^2}\left(\delta\Lambda - \frac{2\delta\kappa\Lambda}{\kappa}\right) = A_0 \tag{82}$$

and

$$-\frac{2}{\kappa^3}\delta\kappa + \frac{1}{\kappa^2}l_0 - \frac{\Lambda}{\kappa^2}(4l_1 + l_2) = B_0, \tag{83}$$

respectively. We assume that the constants A_0 and B_0 now contain the non-vanishing finite pieces introduced by the aforementioned finite renormalization. Equation (83) determines the infinite part of $\delta\kappa$,

$$\delta\kappa = \frac{\kappa}{2}l_0 - \frac{\kappa\Lambda}{2}(4l_1 + l_2) - \frac{\kappa^3}{2}B_0. \tag{84}$$

$\delta\Lambda$ is determined once this result is substituted into Eq. (82):

$$\delta\Lambda = l_0\Lambda - \Lambda^2(4l_1 + l_2) - \frac{\kappa^2}{2}A_0. \tag{85}$$

The counter-terms of the forms $R^2, R^2_{\mu\nu}$ can be absorbed by setting

$$l_1 + \frac{1}{2}l_2 = e_3, \qquad -l_2 = e_4, \tag{86}$$

which yields

$$l_1 = e_3 + \frac{1}{2}e_4, \qquad l_2 = -e_4. \tag{87}$$

Inspection of the coefficients of $F^2_{\alpha\beta}$ implies

$$4l_3 + l_4 = \mathcal{O}(\kappa^4). \tag{88}$$

The coefficients of $RF_{\alpha\beta}F^{\alpha\beta}$ and $R^{\alpha\beta}F_{\alpha\kappa}F_\beta{}^\kappa$ should match with the corresponding coefficients of the counter-term action:

$$l_3 + \frac{l_4}{2} - \Lambda(l_5 + l_6 + 4l_7) - \frac{l_2}{8}\kappa^2 = e_6, \qquad \frac{\kappa^2}{2}l_2 - \Lambda(4l_8 + l_9) = e_5 - e_7 + 2e_8.$$

These constraints are to be combined with those coming from the higher-order counter-terms.

4.3. *Beta function analysis*

In Sect. 4.1 we carried out the analysis without including the cosmological constant. As reviewed therein, dimensional regularization has a technical subtlety: the flat propagator yields vanishing results for the vacuum and tadpole diagrams. For this reason, the shifts in the coupling constants were introduced through finite renormalization. Through the analysis in Sect. 4.2, it has been shown that the cosmological constant is generically generated by the loop effects, and the renormalizability requires its presence in the bare action. This status of the matter suggests the possibility of carrying out an alternative renormalization procedure in which the cosmological constant is included in the starting renormalized action. Once the cosmological constant is included and expanded around the fluctuation metric, the third- and higher-order terms can be treated as a source for additional vertices. The second-order fluctuation term, however, can be treated as the "graviton mass" term.[21] With this arrangement, the vacuum-to-vacuum and tadpole diagrams yield non-vanishing results. In this subsection we carry out the beta function analysis of the vector coupling constant and illustrate this alternative procedure.

An analysis of renormalization of the vector coupling was previously carried out in Refs. [39,40] by employing the setup of Ref. [37]. It was observed that the presence of the cosmological constant generates the formal mass terms for the photon and graviton. Our beta function calculation below yields the same result as Ref. [41].

In the present context, treating a cosmological-constant-type term as the graviton mass term was considered in Ref. [15] for an Einstein-scalar theory with a Higgs-type potential. Let us similarly treat the quadratic part of the cosmological constant term as a formal mass term for the graviton:

$$m^2 = -2\Lambda. \tag{89}$$

For the detailed analysis of the beta function, it is convenient, and common, to introduce a scale parameter μ by making the following scalings:

$$\kappa^2 \to \mu^{2\varepsilon}\kappa^2, \qquad e^2 \to \mu^{2\varepsilon}e^2, \qquad \Lambda \to \mu^{-2\varepsilon}\Lambda. \tag{90}$$

With this, Eq. (1) takes

$$S = \int \sqrt{-\hat{g}}\left(\frac{1}{\kappa^2\mu^{2\varepsilon}}(\hat{R} - 2\Lambda\mu^{-2\varepsilon}) - \frac{1}{4e^2\mu^{2\varepsilon}}\hat{F}^2_{\mu\nu}\right) \tag{91}$$

and one gets, for the kinetic part of the gravity sector,

$$\mathcal{L}_{\text{kin}} = \frac{1}{2\kappa^2\mu^{2\varepsilon}}\sqrt{-\tilde{g}}\left[-\frac{1}{2}\tilde{\nabla}_\gamma h^{\alpha\beta}\tilde{\nabla}^\gamma h_{\alpha\beta} - \frac{1}{2}(-2\Lambda)h_{\mu\nu}h^{\mu\nu}\right]. \tag{92}$$

Treating the cosmological-constant-containing term as the "mass" term modifies Eq. (51) to

$$\tilde{\Delta}(X_1 - X_2) = \int \frac{d^4L}{(2\pi)^4}\frac{e^{iL_{\underline{\delta}}(X_1-X_2)^{\underline{\delta}}}}{i(L_{\underline{\alpha}}L_{\underline{\beta}}\eta^{\underline{\alpha\beta}} - 2\Lambda)}. \tag{93}$$

The correlator relevant for the vector coupling renormalization is

$$-\frac{i}{4\mu^{2\varepsilon}e^2}\int\sqrt{-\tilde{g}}\tilde{F}_{\mu\rho}\tilde{F}_{\nu\sigma}\Big\langle \tilde{g}^{\mu\nu}h^{\rho\kappa}h^\sigma_\kappa + \tilde{g}^{\rho\sigma}h^{\mu\kappa}h^\nu_\kappa - \frac{1}{2}\tilde{g}^{\mu\nu}hh^{\rho\sigma} - \frac{1}{2}\tilde{g}^{\rho\sigma}hh^{\mu\nu}$$

[21] As a matter of fact, we have become aware, after the publication of the present work, of Ref. [41] in which it was noted that the presence of a cosmological constant led to running of the matter coupling constant that was absent when the cosmological constant was not present. It was observed that the cosmological constant acts like mass terms for photon and graviton, a fact independently noted in Ref. [15] for the graviton.

$$+ h^{\mu\nu} h^{\rho\sigma} + \frac{1}{8}\tilde{g}^{\mu\nu}\tilde{g}^{\rho\sigma}(h^2 - 2h_{\kappa_1\kappa_2}h^{\kappa_1\kappa_2})\bigg\rangle. \quad (94)$$

Carrying out the self-contractions of the fluctuation fields, one gets

$$\begin{aligned}
&= -\frac{3i\mu^{2\varepsilon}\kappa'^2}{8\mu^{2\varepsilon}e^2}\int\sqrt{-\tilde{g}}\,\tilde{F}_{\mu\rho}\tilde{F}^{\mu\rho}\int\frac{d^4L}{(2\pi)^4}\frac{1}{i(L^2-2\Lambda\mu^{-2\epsilon})}\\
&= -\frac{3\mu^{2\varepsilon}\kappa'^2}{8\mu^{2\varepsilon}e^2}\frac{\Gamma(\varepsilon)(2\Lambda\mu^{-2\varepsilon})}{(4\pi)^2}\int\sqrt{-\tilde{g}}\,\tilde{F}_{\mu\rho}\tilde{F}^{\mu\rho}\\
&\simeq \frac{3}{32\pi^2(D-4)}\frac{\kappa^2\Lambda}{\mu^{2\varepsilon}e^2}\int\sqrt{-\tilde{g}}\,\tilde{F}_{\mu\rho}\tilde{F}^{\mu\rho},
\end{aligned} \quad (95)$$

where the second equality has been obtained by performing the momentum integration after a Wick rotation. The third equality is obtained by keeping only the pole term in the expansion of $\Gamma(\epsilon)$. The result above implies that the one-loop-corrected vector coupling e_1 is given by

$$e_1 = e\mu^{\varepsilon}\left(1+\frac{3}{8\pi^2(D-4)}\kappa^2\Lambda\right)^{\frac{1}{2}} \simeq e\mu^{\varepsilon}\left(1+\frac{3}{16\pi^2(D-4)}\kappa^2\Lambda\right). \quad (96)$$

From this, it follows that

$$\mu\frac{\partial e_1}{\partial\mu} = \varepsilon e\mu^{\varepsilon} - \frac{3\mu^{\varepsilon}}{32\pi^2}\kappa^2\Lambda\, e. \quad (97)$$

Taking $\varepsilon \to 0$, one gets the following beta function:

$$\beta(e) = -\frac{3}{32\pi^2}\kappa^2\Lambda e. \quad (98)$$

This is the same result as obtained in Ref. [41] because κ^2 in Ref. [41] is twice κ^2 here.[22]

In an earlier related work by Robinson and Wilczek [52], a potentially interesting idea of a shift in the unification scale due to the quantum gravity contributions to the gauge coupling was proposed. The idea was further debated [53–55], and the possibility of quantum electrodynamic (QED) asymptotic freedom was proposed [54]. Before we get to the implications of the present work for these proposals, let us note several technical differences between the beta function analysis of Ref. [52] and the one above.[23] One difference is the use of the traceless/traceful propagator. Another difference is the regularization scheme: momentum cutoff in Ref. [52] vs. dimensional regularization in the present work. For a massless theory certain graphs vanish in dimensional regularization due to the identities

[22] The result in Ref. [41] was obtained by employing the standard one-loop determinant formula. Although, strictly speaking, the formula makes sense only when the traceless part of the fluctuation field is taken out, once the formula is used it does not matter how it was obtained. To rephrase, the result in Ref. [41] was obtained, so to speak, by bypassing the traceful propagator. We believe that this is why the present beta function result, obtained by employing the traceless propagator, agrees with that obtained in Ref. [41]. Incidentally there is a coincidence: it turns out that the result in Eq. (94) remains the same even if one employs the traceful propagator.

[23] The system considered in Ref. [52] is a non-Abelian gauge theory coupled to gravity. For this reason there are more graphs to be considered. For instance, the graph in their Fig. 1, which requires the cubic gauge coupling, does not arise in the present case. If one considers a Higgs-type scalar field as well, then the gauge field becomes massive and the graph should produce an additional contribution analogous to the one obtained in Ref. [54]. For that matter, it will also be interesting to investigate whether and how finite-temperature effects lead to a term analogous to the one obtained in Ref. [54].

such as Eqs. (64) and (68), whereas they do not in momentum cutoff. Still another difference is the gauge fixing.

In the analysis performed in Ref. [54] with the heat kernel method and momentum cutoff, an additional term to the beta function was obtained. The additional term has the same form as the existing term with Λ replaced by a characteristic energy scale square. It then led to potential asymptotic freedom in QED. This proposal, as well as that of Ref. [52], were subsequently debated in Refs. [53,55]. In particular, it was suggested in Ref. [53] that such an additional term will be absent in the de Donder gauge. This suggests the possibility that the potential gauge choice dependence may be responsible for the difference. Given the ξ dependence discussed in Sect. 3.2, we believe that it is a reasonable possibility.

4.4. Scattering predictability and more on 1PI action

It may be useful to recall the case of a non-gravitational theory before considering the gravitational case. Suppose one performed the loop computations and found new vertices required to remove the divergences. In the standard procedure of renormalization, those vertices will be included with the corresponding arbitrary coupling constants in the bare action. If the number of new vertices is finite, the theory is called renormalizable and one proceeds to obtain the 1PI effective action. If the number is infinite, the theory is declared to be unrenormalizable; the infinite number of coupling constants leads to loss of the predictive power of the theory.

In a gravity theory there are an infinite number of counter-vertices, some of which we have seen in Sect. 3. The idea of the field redefinition is that one starts with a bare action of the same form as the classical action with the possible addition of the cosmological constant term. The metric in the bare action is the field-redefined one, $\mathscr{G}_{\mu\nu}$, in Eq. (78). The crucial point is that all of the coupling constants associated with the higher-order counter-vertices are absorbed into the *redefined* metric $\mathscr{G}_{\mu\nu}$, and thus unobservable [51]. The predictability of the theory for scattering amplitudes then follows.

Let us paraphrase. The divergences arising from the loop diagrams can be removed by the counter-vertices present on the right-hand side of the definition of $\mathscr{G}_{\mu\nu}$ in Eq. (78). In other words, with the counter-terms added, the renormalized action now contains all of the new coupling constants. However, the counter-terms with those coupling constants can be combined into Einstein–Hilbert form in terms of the redefined metric $\mathscr{G}_{\mu\nu}$. This means that the bare action has two coupling constants, cosmological and Newton, in terms of the new metric, and therefore the theory is predictive.

More specifically, the theory should become predictive by following the usual “routines”: suppose the experimental values of the cosmological and Newton constants are known accurately to the extent that we may discern the quantum corrections. One can find the values of the renormalized cosmological and Newton constants by imposing certain renormalization conditions. Once the renormalized constants are determined in terms of physical constants, one can proceed to compute, for instance, various scattering amplitudes and make predictions on the corresponding experimental outcomes.

The fact that the infinite number of coupling constants are absorbed by the metric field redefinition must not be taken to mean that the quantum effects are immaterial. All those vertices will be present with fixed finite values of the coefficients in the effective action.[24] At this point one can consider yet

[24] In general, a full effective action is a highly complicated object even containing non-local terms (that may be important for the black hole physics [57]). Here we focus on the starting renormalized action with the added vertices with the fixed finite coefficients.

another field redefinition in conjunction with the quantum deformation of the geometry that plays an important role in the context of black hole information [19,22,56].

5. Conclusion

We have extended the one-loop renormalization of an Einstein-scalar system to an Einstein–Maxwell system. As in the previous works, the amplitude calculations have been carried out with two layers of perturbation in the refined background field method. Since the Maxwell part itself is a gauge system, the extension involves overcoming several additional hurdles. The direct Feynman diagrammatic computation has led to a gauge-choice-dependent 1PI effective action: the effective action is covariant only up to the metric gauge fixing. The origin of the dependence was found in the limitation of the background field method. The proper interpretation of the particular gauge choice independence that we have focused on in this work is that the effective action is made covariant by removing all of the terms containing the gauge-fixing condition. At the same time, the action is to be supplemented by the gauge-fixing condition in the usual manner. We also discussed how the present formalism allows one to avoid or reinterpret the well-known gauge choice dependence. We have taken one step further compared to our previous works: with the fixed renormalization scheme chosen, we have enumerated the quantum corrections of various physical quantities such as the cosmological and Newton constants. The role of the finite renormalization is important. We have seen that the metric field redefinition à la ’t Hooft brings predictive power to the theory.

There are several highlights worth recapitulating. First, note that one ends up taking three different measures to ensure the covariance: removal of the trace part of the metric, employment of the refined BFM, and enforcement of the strong form of the gauge fixing. Second, the cosmological constant has several special features in the context of renormalization. It is the leading term in the derivative expansion, and is generically generated regardless of the background under consideration. Even if one’s starting action does not include the cosmological constant term, the renormalizability dictates its presence in the bare action (and thus in the effective action). Third, the renormalizability requires a metric field definition. The existence of such a field redefinition should not be a coincidence but must be a reflection of the quantum deformation of the geometry. The freedom of such a field redefinition is powerful and distinguishes gravity from non-gravitational unrenormalizable theories.

We have seen that the renormalizability requires the presence of the cosmological term in the bare action. One may take this as a rationale for the presence of a renormalized cosmological constant in the starting renormalized action. In fact, this seems to suggest a future direction that stands out. In the main body we carried out the analysis without including the cosmological constant since we were interested in a flat background. The fact that the cosmological constant is generically generated and required for the renormalizability seems to suggest the possibility that it should be included in the starting renormalized action. This would imply that one should consider the propagator associated with a de Sitter (or anti-de Sitter) background, although the flat spacetime analysis can still be employed for the divergence analysis. Once the cosmological constant is included and expanded around the fluctuation metric, it can be treated as a source for additional vertices.[25]

[25] Alternatively, it can be treated as the “graviton mass” term, and with this the graviton propagator becomes a massive one as we discussed in Sect. 4.3. This may appear too contrived, but the massive propagator makes it unnecessary to introduce the finite renormalization. An objection may be raised that the spacetime is no longer flat in the presence of the cosmological constant term. This is an issue worth exploring further. The bottom line is that the flat space analysis catches the divergences. Also, in a more realistic setup including a Higgs-type scalar, mixing between the physical and unphysical states [58] is expected.

It appears that there are several variant renormalization procedures depending on, e.g., whether or not to include the cosmological constant in the starting renormalized action. As a matter of fact, there is an intriguing possibility when choosing a renormalization scheme. Although the flat space analysis catches the divergent parts of the proper curved space analysis, the finite parts require, in general, the due curved space propagators. One may choose the renormalization scheme such that the finite parts become the same as the corresponding flat analysis. It will be interesting to see whether or not the renormalization procedure could be consistently conducted with such a special scheme. If it could be and yields the same results as the curved space analysis, the flat space analysis will serve as a highly convenient alternative to the proper curved space analysis, and that would imply, in a certain sense, the background independence of the whole framework. Not unrelated, it will be interesting to see whether the aforementioned freedom in the renormalization scheme could be used to absorb the the gauge choice dependence of the coefficients appearing in the action in Eq. (73). (A recent review on such gauge choice dependence can be found in Ref. [60].)

Another direction is the two-loop extension of the results of the present work. As stated in the introduction, the renormalization procedure in this paper is entirely within the standard framework, and in particular the reduction of the physical states did not play a role (other than its role in gauge choice independence and providing assurance that the present procedure can, in principle, be extended to two and higher loops). Although the direct two-loop analysis is expected to be much harder, the difficulty will be of a technical character and associated with computing the Feynman diagrams themselves. One may turn to the approach where the counter-terms are determined by dimensional analysis and covariance [59]. Once the counter-terms are obtained one way or another, it should be possible, with reasonable effort, to extend the field-redefinition-utilized renormalization to two-loop. The reduction to the physical sector [7–9,14], which should be performed after off-shell computation, is expected to play a role at two and higher loops.

Funding

Open Access funding: SCOAP^3.

References

[1] N. D. Birrell and P. C. W. Davies, *Quantum Fields in Curved Space* (Cambridge University Press, Cambridge, 1982).
[2] A. O. Barvinsky and G. A. Vilkovisky, Phys. Rept. **119**, 1 (1985).
[3] I. L. Buchbinder, S. D. Odintsov and I. L. Shapiro, *Effective Action in Quantum Gravity* (IOP Publishing, Bristol, 1992).
[4] V. P. Frolov and I. D. Novikov, *Black Hole Physics: Basic Concepts and New Developments* (Springer, New York, 1998).
[5] J. F. Donoghue, Phys. Rev. D **50**, 3874 (1994) [arXiv:gr-qc/9405057] [Search INSPIRE].
[6] V. F. Mukhanov and S. Winitzki, *Introduction to Quantum Effects in Gravity* (Cambridge University Press, Cambridge 2007).
[7] I. Y. Park, Eur. Phys. J. C **75**, 459 (2015) [arXiv:1404.5066 [hep-th]] [Search INSPIRE].
[8] I. Y. Park, Adv. Theor. Math. Phys. **22**, 247 (2018) [arXiv:1406.0753 [gr-qc]] [Search INSPIRE].
[9] I. Y. Park, Front. Phys. **4**, 25 (2016) [arXiv:1503.02015 [hep-th]] [Search INSPIRE].
[10] I. Park, Universe **5**, 71 (2019) [arXiv:1902.03332 [hep-th]] [Search INSPIRE].
[11] I. Y. Park, J. High Energy Phys. **1504**, 053 (2015) [arXiv:1412.1528 [hep-th]] [Search INSPIRE].
[12] I. Y. Park, Theor. Math. Phys. **195**, 745 (2018) [arXiv:1506.08383 [hep-th]] [Search INSPIRE].
[13] I. Y. Park, J. Math. Phys. **57**, 022305 (2016) [arXiv:1508.03874 [hep-th]] [Search INSPIRE].
[14] I. Y. Park, Int. J. Geom. Meth. Mod. Phys. **14**, 1750092 (2017) [arXiv:1512.08060 [hep-th]] [Search INSPIRE].
[15] I. Y. Park, Eur. Phys. J. C **77**, 337 (2017) [arXiv:1606.08384 [hep-th]] [Search INSPIRE].

[16] I. Y. Park, Fortsch. Phys. **62**, 950 (2014) [arXiv:1304.0014 [hep-th]] [Search INSPIRE].
[17] I. Y. Park, Phys. Lett. B **765**, 260 (2017) [arXiv:1609.06251 [hep-th]] [Search INSPIRE].
[18] F. James and I. Y. Park, Theor. Math. Phys. **195**, 607 (2018) [arXiv:1610.06464 [hep-th]] [Search INSPIRE].
[19] A. J. Nurmagambetov and I. Y. Park, J. High Energy Phys. **1805**, 167 (2018) [arXiv:1804.02314 [hep-th]] [Search INSPIRE].
[20] E. Witten, arXiv:1805.11559 [hep-th] [Search INSPIRE].
[21] I. Y. Park and F. James, Int. J. Mod. Phys. A **29**, 1450047 (2014) [arXiv:1301.6320 [hep-th]] [Search INSPIRE].
[22] I. Y. Park, Class. Quantum Grav. **34**, 245005 (2017) [arXiv:1707.04803 [hep-th]] [Search INSPIRE].
[23] S. Deser and P. van Nieuwenhuizen, Phys. Rev. D **10**, 401 (1974).
[24] G. 't Hooft and M. Veltman, Ann. H. Poincaré Phys. Theor. A **20**, 69 (1974).
[25] V. I. Ogievetsky and I. V. Polubarinov, Ann. Phys. **35**, 167 (1965).
[26] K. Kuchař, J. Math. Phys. **11**, 3322 (1970).
[27] G. W. Gibbons, S. W. Hawking, and M. J. Perry, Nucl. Phys. B **138**, 141 (1978).
[28] P. O. Mazur and E. Mottola, Nucl. Phys. B **341**, 187 (1990).
[29] N. Grillo, arXiv:hep-th/9911118 [Search INSPIRE].
[30] T. Ortin, *Gravity and Strings* (Cambridge University Press, Cambridge, 2004).
[31] S. D. Odintsov, Fortsch. Phys. **38**, 371 (1990).
[32] S. D. Odintsov, Theor. Math. Phys. **82**, 45 (1990) [Teor. Mat. Fiz. **82**, 66 (1990)].
[33] S. D. Odintsov and I. N. Shevchenko, Fortsch. Phys. **41**, 719 (1993) [Yad. Fiz. **55**, 1136 (1992)].
[34] L. Modesto, L. Rachwał, and I. L. Shapiro, Eur. Phys. J. C **78**, 555 (2018) [arXiv:1704.03988 [hep-th]] [Search INSPIRE].
[35] K. Falls, Phys. Rev. D **92**, 124057 (2015) [arXiv:1501.05331 [hep-th]] [Search INSPIRE].
[36] K. Falls, arXiv:1503.06233 [hep-th] [Search INSPIRE].
[37] G. A. Vilkovisky, Nucl. Phys. B **234**, 125 (1984).
[38] E. S. Fradkin and A. A. Tseytlin, Nucl. Phys. B **234**, 509 (1984).
[39] S. R. Huggins, G. Kunstatter, H. P. Leivo, and D. J. Toms Nucl. Phys. B **301**, 627 (1988).
[40] D. J. Toms, Phys. Rev. D **76**, 045015 (2007) [arXiv:0708.2990 [hep-th]] [Search INSPIRE].
[41] D. J. Toms, Phys. Rev. Lett. **101**, 131301 (2008) [arXiv:0809.3897 [hep-th]] [Search INSPIRE].
[42] R. E. Kallosh, O. V. Tarasov, and I. V. Tyutin, Nucl. Phys. B **137**, 145 (1978).
[43] D. M. Capper, J. J. Dulwich, and M. Ramón Medrano, Nucl. Phys. B **254**, 737 (1985).
[44] I. Antoniadis, J. Iliopoulos, and T. N. Tomaras, Nucl. Phys. B **462**, 437 (1996) [arXiv:hep-th/9510112] [Search INSPIRE].
[45] T. R. Morris, SciPost Phys. **5**, 040 (2018) [arXiv:1806.02206 [hep-th]] [Search INSPIRE].
[46] S. Weinberg, *The Quantum Theory of Fields* (Cambridge University Press, Cambridge, 1995), Vol. II.
[47] I. Y. Park, J. High Energy Phys. **1907**, 128 (2019) [arXiv:1811.03688 [hep-th]] [Search INSPIRE].
[48] G. Sterman, *An Introduction to Quantum Field Theory* (Cambridge University Press, Cambridge, 1993).
[49] M. Reuter, Phys. Rev. D **57**, 971 (1998) [arXiv:hep-th/9605030] [Search INSPIRE].
[50] I. Donkin and J. M. Pawlowski, arXiv:1203.4207 [hep-th] [Search INSPIRE].
[51] G. 't Hooft, Nucl. Phys. B **62**, 444 (1973).
[52] S. P. Robinson and F. Wilczek, Phys. Rev. Lett. **96**, 231601 (2006) [arXiv:hep-th/0509050] [Search INSPIRE].
[53] A. R. Pietrykowski, Phys. Rev. Lett. **98**, 061801 (2007) [arXiv:hep-th/0606208] [Search INSPIRE].
[54] D. J. Toms, Nature **468**, 56 (2010) [arXiv:1010.0793 [hep-th]] [Search INSPIRE].
[55] J. Ellis, and N. E. Mavromatos, Nature **479**, E5 (2011).
[56] I. Y. Park, Fortsch. Phys. **65**, 1700038 (2017) [arXiv:1704.04685 [hep-th]] [Search INSPIRE].
[57] V. F. Mukhanov, A. Wipf, and A. Zelnikov, Phys. Lett. B **332**, 283 (1994) [arXiv:hep-th/9403018] [Search INSPIRE].
[58] R. Pius, A. Rudra, and A. Sen, J. High Energy Phys. **1407**, 062 (2014) [arXiv:1401.7014 [hep-th]] [Search INSPIRE].
[59] M. H. Goroff and A. Sagnotti, Nucl. Phys. B **266**, 709 (1986).
[60] P. M. Lavrov and I. L. Shapiro, J. High Energy Phys. **1306**, 086 (2013) [arXiv:1212.2577 [hep-th]] [Search INSPIRE].